Bachelor Thesis

Two Dimensional Analysis of Unknown Gamma-Ray Sources

Katharina Brand

Würzburg, July 24, 2024

Julius-Maximilians-Universität Würzburg
Lehrstuhl für Astrophysik
Betreuer: Prof. Dr. Karl Mannheim

Abstract

To localize new unknown sources or to probe the morphology of sources, a two-dimensional skymap of the gamma-ray events is an important tool. When other telescopes send an alert the position of the source is often not known exactly. By analysing the data not only for the nominal position of the source but also for an area around it, the chance to find the source in the data is increased. In addition, the morphology of an object can only be probed if a larger area around the source is analysed.
A program has been written for the two-dimensional analysis of FACT data. This is then tested with the well-known source Mrk421. It is shown that the source is well visible in the data. However, also some systematic pattern is visible in the skymaps. This can be explained with the analysis method. For specific parts in the skymap, events from the source are misidentified as background. This leads to the observed pattern. One idea of how this can be solved is by subtracting the pattern again from the skymap.
Additionally, the γ-point spread function of FACT is determined using data from the point-like source Mrk421. This can be used to identify extended sources. This is done by comparing the size of the possibly extended source with the size of the point spread function. The PSF width has been determined to be $\sigma = (0.1588 \pm 0.0018)^\circ$.
The other source analysed with the two-dimensional analysis in this work is the galactic centre. Due to the other nearby sources, this is a source predestined for two-dimensional analysis. Besides the analysis of all data at once, additional skymaps with only 2 h of data were produced. Skymaps for a smaller data sample of 2 h do not exhibit any hint of signal. This can be explained by calculating the necessary observation time of about 32 h for the galactic centre.
In the skmaps that are produced with all data (around 33 h after data quality selection) an indication for a source can be found. More data are needed to confirm the detection. The position of the detected excess is compared with the positions of the galactic centre and other nearby sources emitting in the gamma regime. It can be seen that the excess is in agreement with the position of the source Arc, but not with the position of the galactic centre. Nevertheless, the detection of the object Arc is unlikely due to its even fainter brightness compared to the galactic centre. To investigate this further more data of this region are needed.
In the future, more data will be analysed with the two-dimensional analysis, especially data obtained from the follow-up observation of alerts when the source position is unsure. For this, the analysis is going to be optimized and the problems with the artefacts will be solved.

Zusammenfassung

Um neue unbekannte Quellen zu lokalisieren oder die Morphologie von Quellen zu untersuchen, ist eine zweidimensionale Skymap der Gammastrahlenereignisse ein wichtiges Instrument. Wenn andere Teleskope einen Alarm senden, ist die Position der Quelle oft nicht genau bekannt. Indem man die Daten nicht nur für die nominale Position der Quelle, sondern auch für einen Bereich um sie herum analysiert, erhöht sich die Chance, die Quelle in den Daten zu finden. Darüber hinaus kann die Morphologie eines Objekts nur dann untersucht werden, wenn ein größerer Bereich um die Quelle herum analysiert wird.
Es wurde ein Programm für die zweidimensionale Analyse von FACT-Daten geschrieben. Dieses wird dann mit der bekannten Quelle Mrk421 getestet. Es wird gezeigt, dass die Quelle in den Daten gut sichtbar ist. Allerdings sind auch einige systematische Muster in den Skymaps sichtbar. Dies kann mit der Analysemethode erklärt werden. In bestimmten Bereichen der Skymap werden Ereignisse der Quelle fälschlicherweise als Hintergrund identifiziert. Dies führt zu dem beobachteten Muster. Eine Idee, wie dies gelöst werden kann, besteht darin, das Muster wieder von der Skymap zu subtrahieren. Zusätzlich wird die γ-Punktspreizungsfunktion von FACT anhand der Daten der punktförmigen Quelle Mrk421 bestimmt. Diese kann zur Identifizierung ausgedehnter Quellen verwendet werden. Dazu wird die Größe der möglicherweise ausgedehnten Quelle mit der Größe der Punktspreizungsfunktion verglichen. Die PSF-Breite wurde zu $\sigma = (0.1588 \pm 0.0018)^\circ$.
ermittelt. Die andere Quelle, die in dieser Arbeit mit der zweidimensionalen Analyse untersucht wurde, ist das galaktische Zentrum. Aufgrund der anderen nahegelegenen Quellen ist diese Quelle für die zweidimensionale Analyse prädestiniert. Neben der Analyse aller Daten auf einmal wurden zusätzliche Skymaps mit nur 2 h an Daten erstellt. Skymaps für eine kleinere Datenstichprobe von 2 h zeigen keine Anzeichen eines Signals. Dies lässt sich durch die Berechnung der notwendigen Beobachtungszeit von etwa 32 h für das galaktische Zentrum erklären.
In den Skmaps, die mit allen Daten (etwa 33 h nach Datenqualitätsselektion) erstellt werden, lässt sich ein Hinweis auf eine Quelle finden. Um den Nachweis zu bestätigen, werden weitere Daten benötigt. Die Position des entdeckten Überschusses wird mit den Positionen des galaktischen Zentrums und anderer nahegelegener Quellen verglichen, die im Gammabereich emittieren. Es zeigt sich, dass der Überschuss mit der Position der Quelle Arc übereinstimmt, aber nicht mit der Position des galaktischen Zentrums. Dennoch ist der Nachweis des Objekts Arc unwahrscheinlich, da es im Vergleich zum galaktischen Zentrum noch schwächer leuchtet. Um dies weiter zu untersuchen, werden mehr Daten aus dieser Region benötigt. In Zukunft sollen mehr Daten mit der zweidimensionalen Analyse ausgewertet werden, insbesondere Daten aus der Nachbeobachtung von Alarmen, wenn die Position der Quelle unsicher ist. Hierfür wird die Analyse optimiert und die Probleme mit den Artefakten werden gelöst werden.

Contents

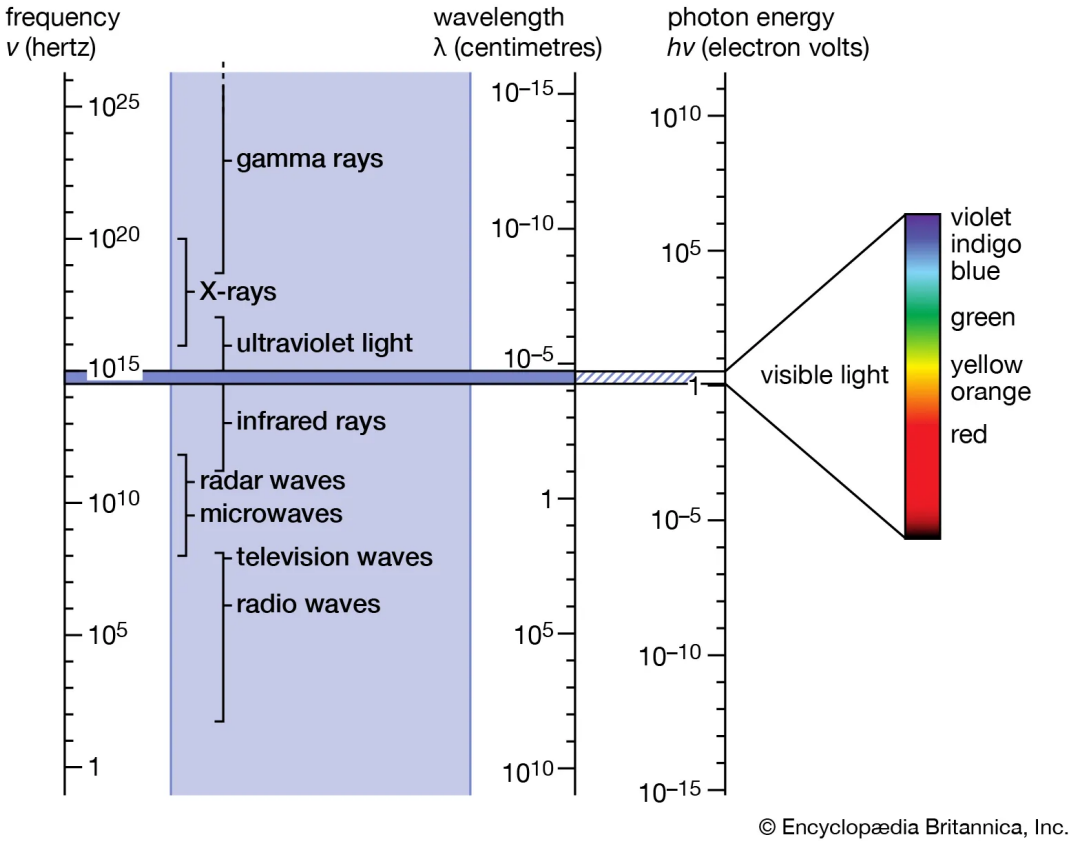

Figure 1: The electromagnetic spectrum is shown. For each region the name, the frequency range, the wavelength and energy range are displayed. The visible range is displayed magnified on the right side. The figure was taken from [1].

1 Scientific Background

The electromagnetic spectrum (Figure 1) ranges from radio waves with wavelengths of several kilometres and energies in the neV range to gamma rays with wavelengths less than pm and energies from 500 keV to more than several TeV.
In the following gamma rays, the most energetic part of the electromagnetic spectrum at the top in Figure 1, is explained. In addition, the principle of telescopes measuring gamma rays is shown, along with some information about the telescope used to take the data analysed in this paper.

[1] https://www.britannica.com/science/electromagnetic-spectrum

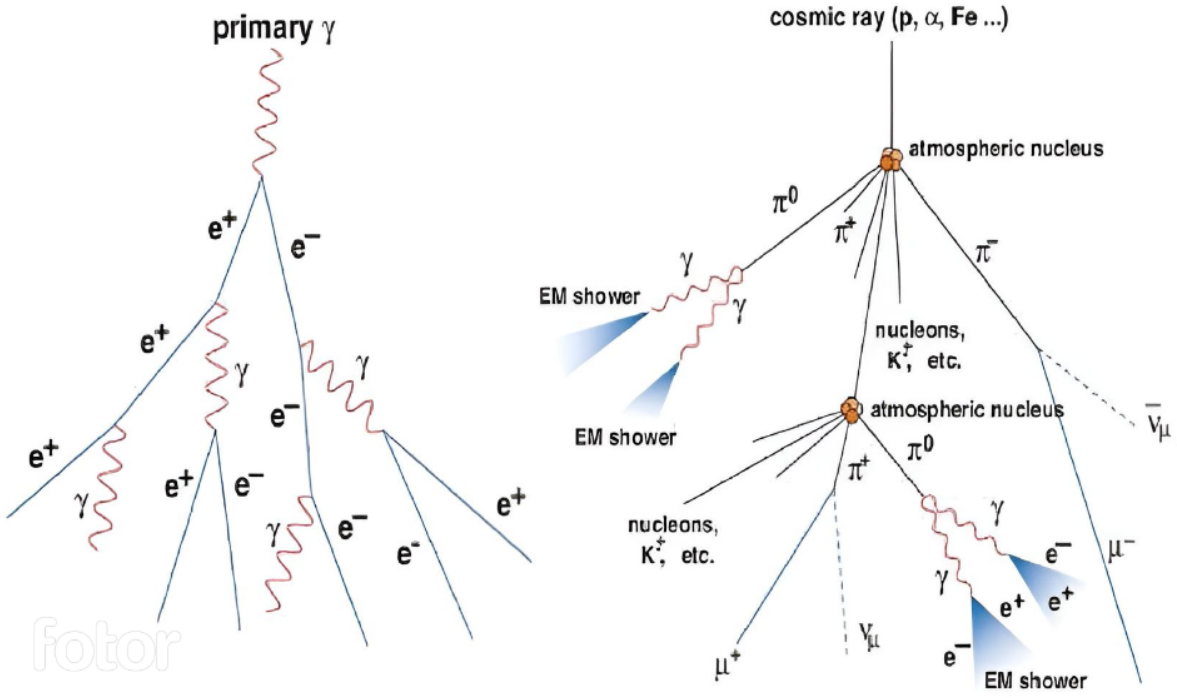

Figure 2: The left scheme shows the evolution of the shower with a γ photon as the primary particle and the right scheme with a cosmic ray as the primary particle. The figure was taken from López-Oramas, A. 2015.

1.1 Production of Cherenkov Radiation

The information in the following sections can be found in Schönfelder, V. 2001 and Weekes, T. C. 2003. The gamma-ray spectrum can be divided into two parts. The first one can only be observed from space, with an energy range from 500 keV to 100 GeV. This part is not relevant for this work and will not be discussed further. The second part, with energies around 100 GeV and higher, is observed indirectly from the Earth's surface.

1.1.1 Interaction of gamma photons with the atmosphere

For a gamma photon with an energy greater than 10 MeV the dominant interaction in matter is pair production. So when such a gamma photon hits the atmosphere it undergoes pair production at an altitude of around 20 km above sea level. This can also be seen in Figure 2 on the left. This pair shares the total energy of the primary gamma photon. The emission angle α of the process is proportional to

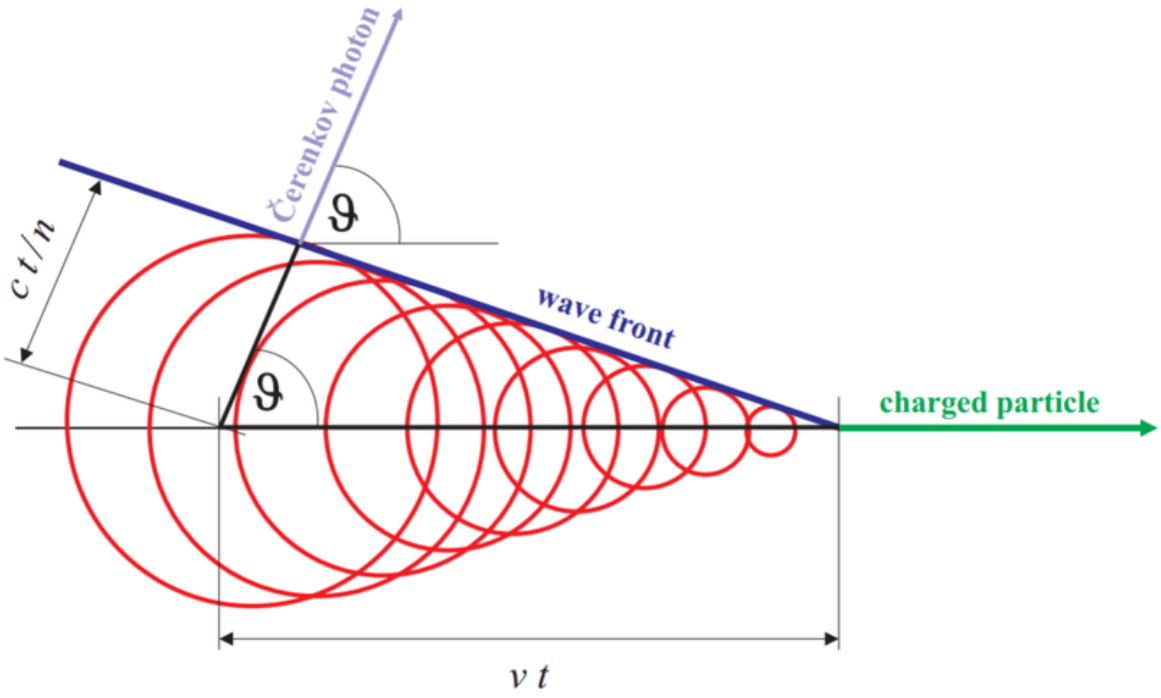

Figure 3: Shown is a scheme of the geometry of Cherenkov radiation. The charged particle moves at a velocity $v > c_n$, where c_n is the speed of light in the medium. The normal vector of the surface of the generated wavefront encloses an angle of ϑ with the direction of the particle. The figure was taken from Hrupec, D. 2008.

$$\alpha \propto \frac{m_e c}{E}, \tag{1}$$

with m_e the rest mass of the electron or positron, c the speed of light in vacuum and E the energy of the photon. Due to the high energy of the primary particle, the pair is emitted in the direction of the velocity of the primary particle.

The produced electron-positron pair then interacts with the molecules in the atmosphere via bremsstrahlung and produces secondary gamma-photons, as can be seen in Figure 2 on the left. These secondary photons can then again produce new electrons and positrons via pair production. These processes continue until the energy of the particles falls below a certain threshold, where the ionisation losses are equal to the radiation losses. The scheme of such a shower is shown in Figure 2 on the left. For comparison, the scheme of a shower produced by a cosmic ray, such as a proton, as a primary particle is shown on the right of Figure 2. It can be seen that cosmic rays produce a greater variety of particles over a

larger area.

1.1.2 Cherenkov radiation

If the produced secondary electrons and positrons have a velocity greater than the speed of light in the atmosphere

$$v > \frac{c}{n}, \tag{2}$$

they produce Cherenkov radiation. Here, v is the velocity of the particle, c is the speed of light in vacuum and n is the refractive index of the atmosphere. The opening angle ϑ of the Cherenkov cone depends on the velocity v of the particle that produced the Cherenkov radiation via:

$$cos\,\vartheta = \frac{1}{\beta n} \tag{3}$$

with $\beta = \frac{v}{c}$. This geometry of Cherenkov radiation can also be seen in Figure 3. In this figure, the elementary Cherenkov waves produced by the charged particle are shown in red. It is also visible how they expand with time and form a wavefront together. The norm of this wavefront encloses an angle of ϑ together with the direction of the charged particle. With this, equation 3 can be derived from Figure 3 with some geometry.
According to Schönfelder, V. 2001, about 50 $\frac{ph_C}{m^2}$ are produced in total in the shower of a primary gamma ray of about 1 TeV. With ph_C being the number of Cherenkov photons. A Cherenkov flash of one primary gamma photon lasts approximately 5 ns. The area of the Earth's surface that gets hit by the photons has a radius of about 100 m (also marked in Figure 4).

1.2 Imaging Atmospheric Cherenkov Telescopes

This section is based on Schönfelder, V. 2001 and Weekes, T. C. 2003. The Cherenkov radiation explained in the last Section 1.1 can be observed with **I**maging **A**ir **C**herenkov **T**elescopes (IACTs), as shown in Figure 4. IACTs use the whole atmosphere as a sensitive material, since the detected Cherenkov radiation is produced in a large volume of the atmosphere (upper part of Figure 4). In Figure 4 also the area of the Earth's surface which gets hit by the Cherenkov radiation from a single primary gamma particle, is visible. If an IACT is standing in this area, it can detect parts of the Cherenkov radiation and record an image similar to the one on the right side of Figure 4. The information obtained from the image can be used to reconstruct the parameters of the primary particle.

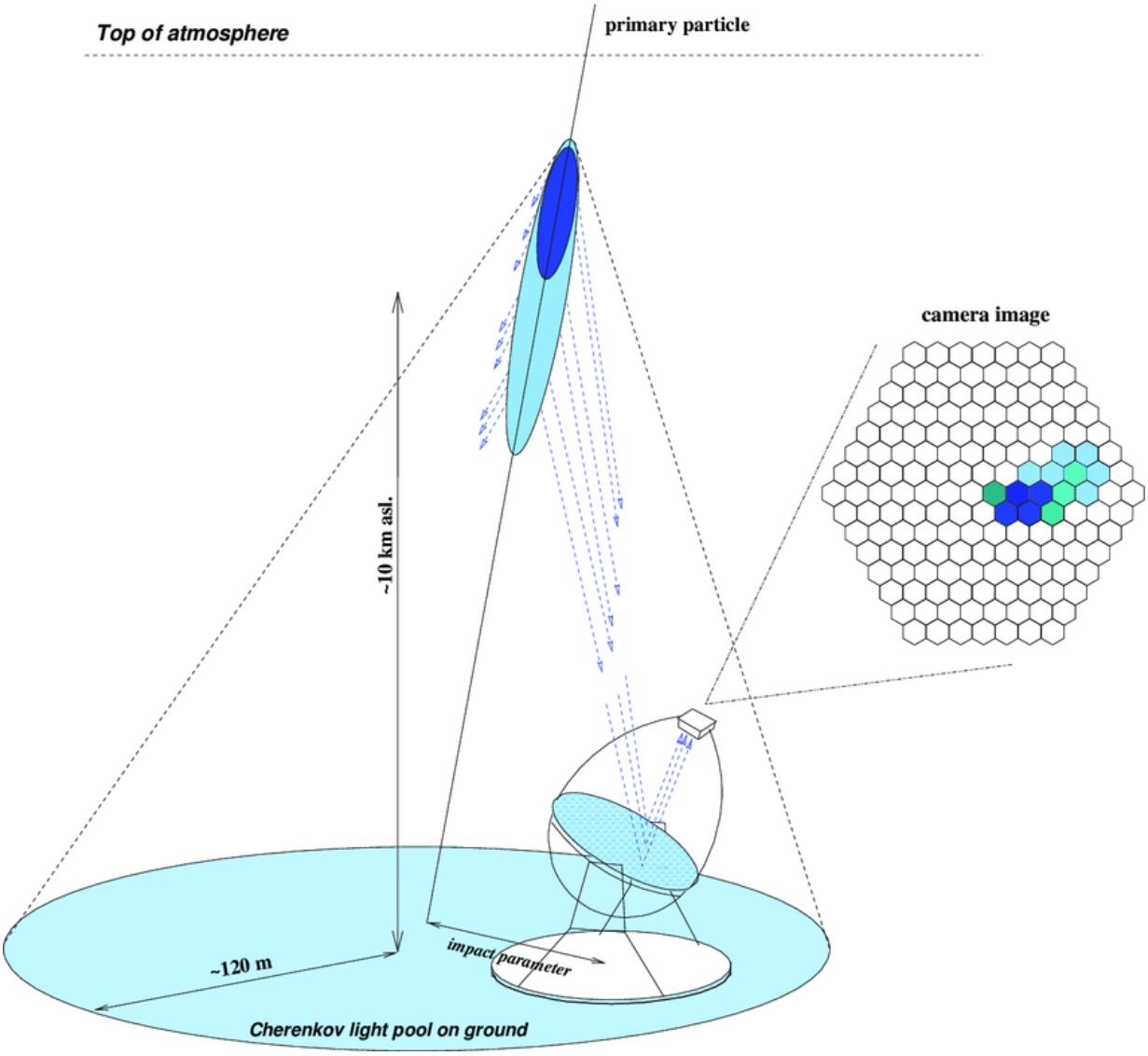

Figure 4: The scheme shows the Cherenkov light from the shower hitting the Earth. The area hit by the Cherenkov light is marked by the turquoise circle. The telescope standing in this area catches parts of the light and records the shown image. The figure is taken from Lopez, M. et al. 2009

The spectrum of the produced Cherenkov photons peaks in the blue to near-UV region. **P**hoto-**M**ultiplier-**T**ubes (PMTs) sensitive in the optical regime are therefore sufficient to detect this radiation. The main parts of such a telescope are therefore a large mirror to collect the Cherenkov photons and the light detector, often a PMT, in the focal plane of the mirror. In addition, the camera (PMT) must be connected to the fast pulse-counting

electronics, due to the short duration of the pulse.
Since the telescopes detect the Cherenkov photons, but information about the primary gamma photons is searched, the conditions under which the Cherenkov photons were produced should be known as precisely as possible. It is therefore very important to know the conditions in the atmosphere as accurately as possible because the atmosphere is the sensitive material. Parameters such as temperature, pressure and humidity are monitored. Of course, these parameters are not completely accurate and do not apply to the entire atmosphere. Due to the lack of knowledge of the precise conditions within the atmosphere, Monte Carlo simulations are needed to reconstruct the parameters of the primary particle.

1.3 The First G-APD Cherenkov Telescope

This section is based on [2], Anderhub, H. et al. 2013b and Dorner, D. et al. 2015. The most existing IACTs use **p**hoto**m**ultiplier **t**ubes (PMTs) as detectors. One of the disadvantages of PMTs is that they are easily damaged by excessive light, such as the full moon. This leads to observational gaps of several days a month. So PMTs are not very suitable for long-term observations of variable sources, where it is crucial to have continuous observations to detect the variability.
To test a new type of detector that is less sensitive to excessive light exposure, the **F**irst G-**A**PD **C**herenkov **T**elescope (FACT) was built. As detector a silicon-based photosensor, consisting of 1440 solid-state photosensor **G**eiger-mode **A**valanche **P**hoto**d**iodes (G-APDs) with the described advantage, is used. The camera was mounted on the substructure of the former HEGRA CT3 telescope to keep the costs as low as possible, as FACT's primary purpose was to test the new 1440 pixel camera.
The telescope is located on the Canary Island of La Palma at 2200 m a.s.l. Due to the high location clouds are usually beneath the telescope creating good observation conditions. Observation, to test the camera, started in the autumn of 2011. Since then gamma photons have been observed by FACT in the energy range from several hundred GeV to about 10 TeV. Besides the task of proving the advantage of G-APDs, the physical program is the long-term observation of bright **a**ctive **g**alactic **n**uclei (AGNs) and bright TeV blazars, due to their high variability of these.
The most frequently observed objects by FACT are Mrk421 and Mrk501. This is also one of the reasons why data from Mrk421 were used to test the two-dimensional analysis described in Section 3. The results are presented in Section 4.
Additionally to the long-term observation of a few bright sources, FACT also reacts to

[2] https://www.isdc.unige.ch/fact/facts

Figure 5: A picture of the First G-APD Cherenkov Telescope is shown. The picture was taken from Anderhub, H. et al. 2013a.

alerts from other telescopes. These notifications are sent for example when a new source is identified in the data, and it is intended that other telescopes observe this source, especially at different wavelengths. The data produced by FACT during such observations are predestined to be analysed by the two-dimensional analysis described in this work. This topic is further discussed in the next section.

All the data analysed in this work were taken in the so-called Wobble mode. In this mode, the position of the source called ON is not in the centre of the telescope but has a small offset. This can be seen in Figure 6. For FACT, the offset is 0.6° Dorner, D. et al. 2013. Besides the ON position, five other positions are defined so that all six are symmetrical regarding the centre of the telescope. This is shown in Figure 6. From these positions,

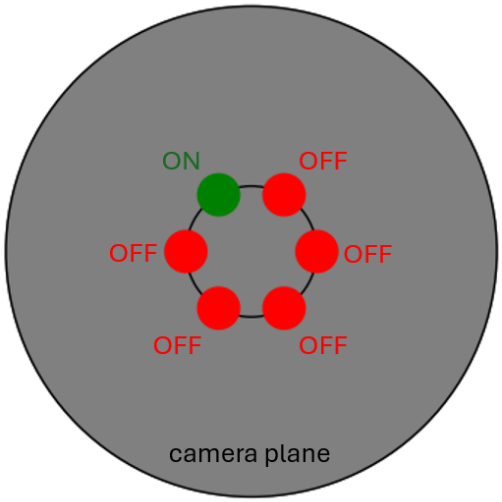

Figure 6: A scheme of the camera plane is visible. The ON and OFF positions, for which the data are analysed, are shown. The distance of each position to the centre and the distance between neighbouring positions is 0.6 °. The radius of one position is 0.19 °, due to the θ^2-cut chosen in this work. This figure is based on Pfahler, L., Bunse, M. and Morik, K. 2021.

called OFF positions, the background is determined. The telescope must be positioned so that there are no known sources at the background positions, as they are used to determine the statistical background that needs to be subtracted from the ON data to obtain the number of data from the source itself. This allows the source and the background to be observed simultaneously. This helps to reduce uncertainties due to different observing conditions between the source and background data.
Furthermore, the telescope rotates every twenty minutes so that the position of the source in the camera plane changes by 180°. This means that looking at Figure 6 the ON position swaps position with the opposite OFF position every twenty minutes.

```
////////////////////////////////////////////////////////////////////////
TITLE:            GCN/AMON NOTICE
NOTICE_DATE:      Wed 29 May 19 01:55:49 UT
NOTICE_TYPE:      AMON ICECUBE HESE
RUN_NUM:          132628
EVENT_NUM:        41485283
SRC_RA:           287.3190d {+19h 09m 17s} (J2000),
                  287.0754d {+19h 08m 18s} (current),
                  287.9377d {+19h 11m 45s} (1950)
SRC_DEC:          +78.1432d {+78d 08' 36"} (J2000),
                  +78.1751d {+78d 10' 31"} (current),
                  +78.0589d {+78d 03' 32"} (1950)
SRC_ERROR:        534.00 [arcmin radius, stat+sys, 90% containment]
SRC_ERROR50:      96.00 [arcmin radius, stat+sys, 50% containment]
DISCOVERY_DATE:   18632 TJD;   149 DOY;   19/05/29 (yy/mm/dd)
DISCOVERY_TIME:   6922 SOD {01:55:22.21} UT
```

Figure 7: The notification from a received alert is shown. A red box marks the uncertainty in the location of the alert position together with the containment level. The image was adapted from [3].

2 Multimessenger Astrophysics

As already discussed in Section 1.3, FACT is an IACT. These types of Cherenkov telescopes are pointing telescopes. This means that they can only point at one point in the sky and therefore cannot observe the entire visible night sky, but only a very small part around the pointing position, depending on the Field of View. In comparison, telescopes such as the **H**igh-**A**ltitude **W**ater **C**herenkov Gamma-Ray Observatory (HAWC)[4] are all sky telescopes that observe a large part of the visible night sky at once, with a very different observing method further described in Abeysekara, A. U. et al. 2017.

It was also mentioned in 1.3 that one of the main goals of FACT is the long-term observation of bright TeV blazars. However, sources emit light not only in one waveband but rather across the whole electromagnetic spectrum and may also emit neutrinos and gravitational waves. To observe the connection between the different wavebands and messengers, it is important to perform joint multiwavelength observations and react to alerts sent by other telescopes. Furthermore, FACT also sends out alerts to other telescopes. The possible object addressed in the alert is also called **T**arget **o**f **O**pportunity (ToO).

For example, if FACT receives a ToO via the **A**stropysical **M**ultimessenger **O**bservatory **N**etwork (AMON)[5] from another telescope such as IceCube, the message looks approximately like Figure 7. Besides all the general information like the title and who sent the

[3] https://gcn.gsfc.nasa.gov/notices_amon/41485283_132628.amon

[4] https://hawc-observatory.org

[5] https://www.amon.psu.edu

alert, the interpolated position of the source is also given. It is important to mention the displayed errors, marked with a red square. The errors are provided in arcminutes (arcmin) for a containment of 90% and 50%. This means that the source is with a probability of 90% respectively 50% inside a circle with the error as radius. The values offered in arcmin correspond to 8.9° radius for 90% and 1.6° radius for 50%.
With a **F**ield **o**f **V**iew (FoV) of 4.5° diameter[6], FACT can observe the whole area inside the 50% containment of the example above when pointed in the centre but not the whole area of the 90% containment. When the source is not directly at the stated position with the highest probability, but rather somewhere else more in the outer part of the area, the source could not be detected by the FACT telescope and nothing is visible in the data.
The second problem is that the current analysis of the data can only analyse the data for one position. So even if the Field of View is large enough, for example, if the source is inside the 50% containment, the source will not be detected in the analysis.
Additionally, not all sources are point-like and the current analysis cannot survey the morphology of an object. As FACT has mainly observed point-like objects a two-dimensional analysis was not needed. For the few possible, extended sources, a simple analysis is not sufficient. For them and sources with an uncertain position, a two-dimensional analysis is needed.
With a two-dimensional analysis, it would be possible to see the source and also the extension, as long as it is in FACT's Field of View. For this purpose, the code of the already automated analysis can be used as a basis together with a loop. The loop is used to calculate new possible source positions in a grid with a defined step width in the focal plane of the telescope. For each position, the events are analysed and the events coming from that theoretical source position are identified. The number of these events can be used to calculate the significance of each position. Finally, this is plotted to visualise everything.
In addition, extended sources can be identified by comparing their size to the size of the γ-**P**oint **S**pread **F**unction (γ-PSF). The γ-PSF is instrument-dependent and can be determined with a point-like source. The code is described in Section 3.
The code is tested on a very well-known point-like source, Mrk421, to verify the functionality. The results are presented in Section 4. The code is used to analyse data taken from the Galactic Center (Section 5). This is also an interesting test for the camera and preanalysis parts of FACT, as other sources near the Galactic Center, emitting in the gamma or optical blue regime, could interfere the observation.

[6] https://www.isdc.unige.ch/fact/facts

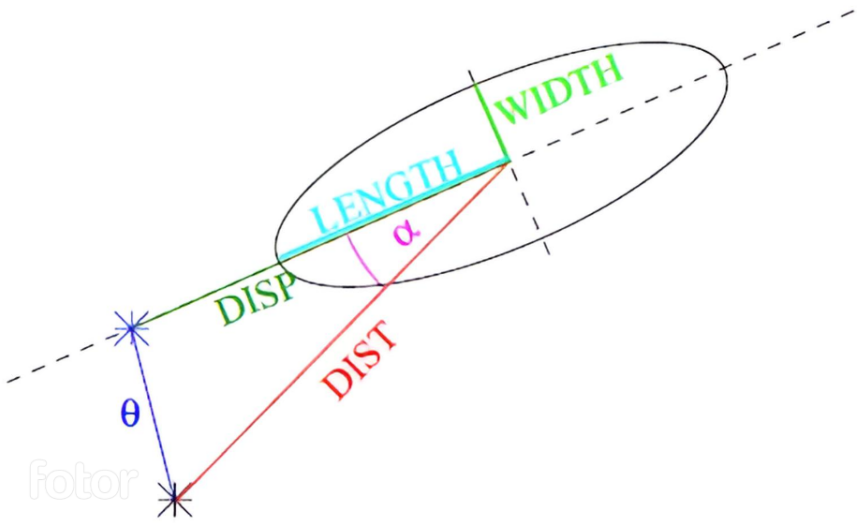

Figure 8: The ellipse indicates the event in the camera. The width and length of the ellipse are defined. By reconstructing the origin of the event, DISP is defined. DIST is the distance from the centre of gravity of the ellipse to the source position. The angle between DIST and DISP is θ. The Figure was taken from Lehrstuhl für Astronomie 2018.

3 Data Analysis

In this bachelor thesis, data are analysed with a two-dimensional analysis to identify sources even though they have a deviating source position compared to the position stored in the database. The program written for this purpose is explained in this section.
The program is divided into several parts. The SQL script is embedded in the shell script. It calculates the new source positions and thus a θ^2 value for each event. Then the significance values for each part in the skymap are calculated using two ROOT macros. Furthermore, this is plotted using another ROOT macro. First of all the general analysis of FACT is explained.

3.1 FACT Analysis

This section is based on Dorner, D. et al. 2015. Like the fully automated operation of the FACT telescope, the analysis is also fully automated, except for the spectra calculation. The received data are stored in a SQL database.
The events are analysed and processed using the **M**odular **A**nalysis and **R**econstruction **S**oftware (MARS). The first step is signal extraction and calibration. In this step, the signal is extracted and bad pixels are interpolated with the information from the neighbouring

pixels.
The next step, described in Arbet-Engels, A. et al. 2021, is the image cleaning. This is done for each event. Here, all the pixels with noise are removed from the images. Two sub-steps are performed. First, the difference in arrival time of neighbouring pixels is used to define islands. If the difference is less than 2.4 ns, the pixels are joined to an island. Additionally, adjoining islands are also joined. Second, if these defined islands have a total signal of less than 25 pe (photon equivalents), they are rejected. After that, the image parameters Width W, Length L, Size S, Slope ΔT and the centre-of-gravity $\vec{P}$ are calculated, as mentioned in Beck, M. et al. 2019.
During this data processing, the database (described in Schleicher, B. et al. 2022) is automatically filled on an event basis with the image parameters. In addition, the database is used to store all relevant data on a run-wise basis.
Furthermore, data-quality selection cuts based on the cosmic-ray rate are applied on a run basis, as described in Arbet-Engels, A. et al. 2021 and further introduced in Hildebrand, D. et al. 2017. For this, the parameter $R750$ is introduced, as the artificial trigger rate above the threshold of 750 DAC-counts. It is chosen to be independent of the trigger threshold and the night sky background. But the value is dependent on the zenith distance and needs to be corrected for that, leading to $R750_{corr}$. The zenith distance dependency is further described in Bretz, T. 2019 and Mahlke, M. et al. 2017. Due to seasonal changes in the cosmic-ray rate, a reference value ($R750_{ref}$) for each moon period is determined. The ratio $R750_{corr}/R750_{ref}$ of good quality data (good weather) can be described with a Gaussian distribution. Bad weather data can be identified and removed based on a deviation from the Gaussian distribution. Therefore $R750_{corr}/R750_{ref}$ is chosen to be between 0.93 and 1.3 in this work. The parameter is listed in Table 1.
Afterwards, the background suppression is done on an event basis. This is completed with SQL queries in the database. Before that, all events for which the reconstruction of the event origin is not possible or not good enough are removed. The position cannot be reconstructed sufficiently if the event consists of less than five pixels (parameter NumUsedPixels), has more than three islands or has a too high percentage of the signal in the outer part of the telescope (parameter Leakage1). If the Leakage1 value is too high one can assume that a huge part of the event is outside of the camera, which makes the reconstruction difficult. The quality cuts applied are also shown in Table 1. The chosen values in this work are 5.5 for NumUsedPixels and 0.1 for the Leakage1 value.
Then the image parameters that are filled into the database are used to reconstruct the origin, energy and type of the primary particle. Therefore, the disp and dist values are calculated. The definition of the values is illustrated in Figure 8. To estimate the origin

of the primary particle, the disp method, described in Lessard et al. 2001, is used. Disp is the angular distance from the centre of gravity to the reconstructed origin of the gamma ray. It is calculated after Beck, M. et al. 2019:

$$disp = \left(1.29^\circ + 60\text{ps} \cdot \frac{\Delta T}{ns/^\circ} + 4.26^\circ \cdot l\right) \cdot \left(1 - \frac{W}{L}\right). \tag{4}$$

After Beck, M. et al. 2019, the disp value is optimized with data from the Crab Nebula from winter 2017/18. It is chosen such that it has the smallest relative errors on the measured excess. This needed to be kept in mind when talking about the γ-PSF of FACT, as the size of the γ-PSF is dependent on the parametrization of disp.
Dist is however the angular distance from the center of gravity to the position of the source in the image plane. With these values, θ (Figure 8) and also θ^2 can be calculated. So θ^2 indicates the angle between the position of the source and the reconstructed origin of the event. These values are used to calculate the excess-rate curves in the final step. The further steps for the two-dimensional analysis are described in the next sections.

3.2 The User Input

The basis of the program is a shell script, in which the loops for calculating the different assumed source positions are implemented. A third loop handling the data on a nightly basis allows for parallelizing the process.
First, the user is prompted to fill in the input parameters. The area in which the positions are to be calculated is required. Starting from the nominal source position, the angle in degrees for Right Ascension (RA) and Declination (DEC) is requested. In addition, the increment (step width) is required, which defines the distances at which new source positions are calculated. As there is Right Ascension and Declination, two loops are needed to cover all possible combinations. The specified range of angle with increment is used to calculate the start and end position values for the loops. Furthermore, the user-defined time interval, that should be analysed, is passed to the third loop.
The next required values are the paths and names of the two files to be saved. The first file stores the calculated data (number of ON and OFF events, significance). In the second file, the plot is saved which was calculated from the data. The storage locations are passed to the ROOT macro part where it is needed.
The last needed values are the ones for the data selection, data-quality selection cuts and quality cuts. The user never wants to analyse all the data and for a reliable result also only good quality events should be used. Therefore, only data from the selected source in the chosen time interval and with good quality, meaning good weather as described in the last

name in FACT database	format	type	explanation
fSourceKey	integer	value	the source to analyse
fNight	yyyy-mm-dd	range	time interval to analyse
NumUsedPixels	decimal number	minimum	number pixels in an event
Leakage1	decimal number	maximum	proportion of the event in the outer part of the camera
fR750Cor/fR750Ref	decimal number	range	quality of the data (weather)

Table 1: The names of the needed parameters are displayed. The parameters are used for data selection (first two), to check the data quality on the event basis (third and fourth) and as data-quality selection cuts on the run basis (last value). Additionally, the format and type for each parameter are listed. An explanation for each parameter is given.

section, are selected. The parameters, for which cuts are used, the format and the type are given in Table 1. The first two parameters in Table 1 specify the source and time, with the fSourceKey being the unique identification of each source and the fNight values giving the time interval in which the data should be analysed. The next two parameters are used for quality cuts as described in Section 3.1. The last value is for the data-quality selection cut and is also described in Section 3.1. The values for the cuts are passed to the SQL script described in the next section.
The SQL script is automatically generated each time a new iteration of the innermost loop is started, as the new values need to be implemented. The new SQL script is then executed.

3.3 Calculation of the Position and θ values

The coordinates of the sources are usually given in a celestial coordinate system since the position is then independent of the position on Earth and also independent of source movements compared to the Solar System, as the position is defined for a specific date. The positions of the sources observed by FACT are stored with the coordinates in a celestial coordinate system in the database. However, to determine whether an event came from the source, the position must be transformed to the focal plane of the telescope via the horizontal coordinate system. The different coordinate systems are described below in order to understand what the SQL code does in this part of the program.

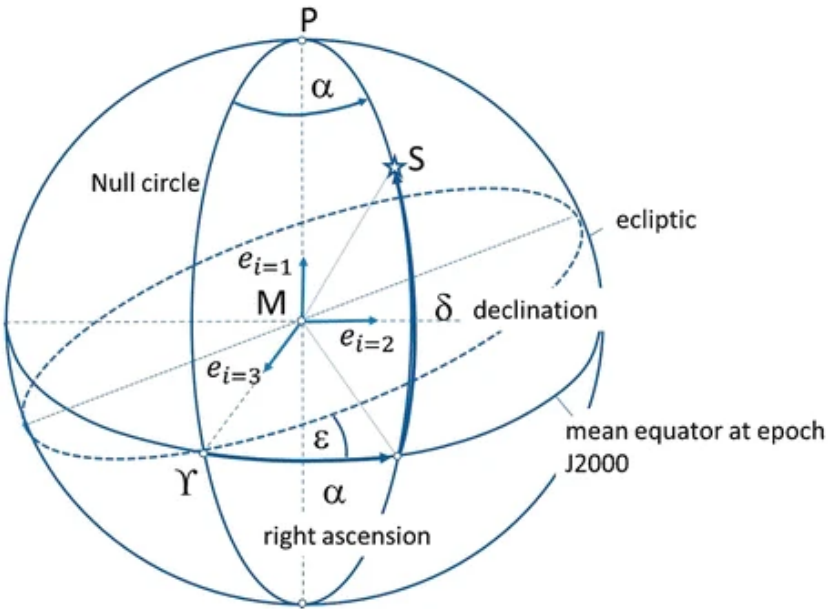

Figure 9: A scheme of a celestial coordinate system according to the ICRS is visible. All objects are displayed in a sphere around the origin M, the barycentre of the solar system. The Declination δ is defined as the distance of the star S from the equatorial plane at a given time, here the 1. January 2000 at 12 pm terrestrial time (TT). The Right Ascension α is defined in the equatorial plane as the distance of the projection of the star to the equatorial plane and the point where the equator and ecliptic cross (Υ). This Figure is taken from Seitz, M. et al. 2015.

3.3.1 The International Celestial Reference System

Information about the ICRS is taken from [7]. The origin of the International Celestial Reference System (ICRS) is the barycentre of the Solar System and is therefore independent of the position of the telescope on Earth. The axes are "space fixed", meaning that they do not rotate with respect to distant objects in the Universe. They are used to describe the positions of distant celestial objects.
The fundamental plane defined in the ICRS is the extension of the Earth's equatorial plane at a given date. In Figure 9 it is marked as mean equator at epoch J2000'. The Declination δ is defined as the angular distance from this plane to the North or South, also visible in Figure 9. Right Ascension, on the other hand, is defined as the angular distance measured eastward along the equatorial plane from a defined reference point. The reference point used is the equinox point Υ. This is the point where the Sun crosses the equatorial plane

[7] https://aa.usno.navy.mil/faq/ICRS_doc

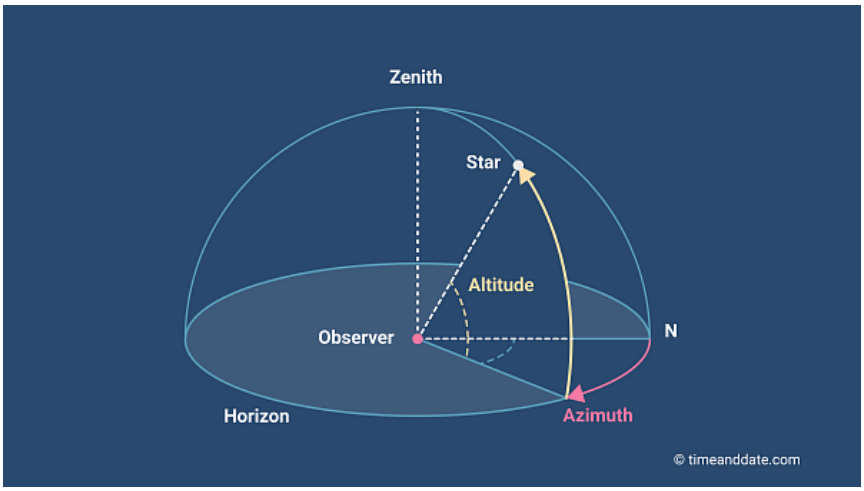

Figure 10: Visible is a scheme of a horizontal coordinate system. All objects are displayed in a sphere around the observer. The horizon of the observer defines the plane. Altitude is defined as the distance between the star S and the horizon plane. Azimuth is defined in the horizon plane as the distance from the North direction N to the projection of the star onto the plane. The Figure is taken from Bikos, K. n.d.

in its annual path from South to North. The Sun's motion lies in the ecliptic plane, also visible in Figure 9. Since both the equatorial and ecliptic planes move with respect to time, the coordinate system must be defined for a particular date. In the case of Figure 9 and also of the FACT data, this date is 1.1.2000 at 12 pm terrestrial time (TT).

3.3.2 The Horizontal Coordinate System

The horizontal coordinate system provides the direction in which the object is found, depending on the position of the observer. In this system, the sky is defined as a dome, with the observer at the centre of the ground plane and the edges at the horizon. This can be seen in Figure 10. The observer plane is defined as the plane perpendicular to the direction of gravity at the observer's location. The azimuth angle is defined from the North direction to the projection of the object on the horizon, so the azimuth values increase towards the east. Whereas the altitude angle is defined as the angle the object makes with the ground plane. This means that an object visible on the horizon has an altitude angle of 0 °. The altitude angles below the horizon are therefore negative. Instead, the zenith distance, defined as the angle between the surface normal and the star, can be used. The surface normal is defined from the observer position.
It is also important to note that objects move across the sky. This means that the coordi-

nates of an object in this coordinate system are time-dependent.

3.3.3 The Calculation

From the horizontal coordinate system, the positions are transformed into a Cartesian coordinate system representing the camera plane. If standing at the dish of the telescope looking at the camera, the x-axis is defined to the right from the centre of the dish. The y-axis is defined from the same point upwards.
These coordinate transformations are also already done in the automated analysis, and the code presented here is largely based on it. The main difference is that the automated analysis is written in C++ and this part of the analysis is here written in SQL. The advantage of writing in SQL is that direct access to the data is possible as on an event basis all Image Parameters are stored in the database.
When the source position is transformed onto the camera plane, the θ^2, in the following also ThetaSq, value is calculated for each event with respect to the source position. Furthermore, a θ^2 value is also calculated for each event concerning each background position. So one gets six times each event just compared to different positions and therefore with different θ^2 values. This is repeated in each loop cycle, i.e. for each calculated possible source position, for all events. The value of θ^2 is an indication of whether the gamma photon came from that particular position. In the following section, all events with a too-large $theta^2$ are discarded, as they are identified as not coming from that position.

3.4 Calculation and Plotting of the excess and significance values

The data returned by the SQL code can be used to calculate the excess and significance values. These calculations are done using ROOT[8]. First, all events with a θ^2 value greater than 0.037 are discarded. These values are discarded because a large θ^2 means that the distance between the reconstructed position of the event and the source position or the background position is large. This can also be seen in Figure 8.
The remaining duplicated events are sorted into two groups (ON and OFF), depending on the position for which the θ^2 value is calculated. How the ON and OFF positions are distributed on the camera plan is shown in Figure 6. The number of ON and OFF events is determined and for one source position all ON and OFF events from all analysed days are

[8]Rene Brun and Fons Rademakers, ROOT - An Object Oriented Data Analysis Framework, Proceedings AIHENP'96 Workshop, Lausanne, Sep. 1996, Nucl. Inst. & Meth. in Phys. Res. A 389 (1997) 81-86. See also "ROOT" [software], Release v6.26/06, 28/07/2022. https://root.cern/releases/release-62610/#retracted

summed. The number of ON and OFF events (N_{ON} and N_{OFF}) for each source position is then used to calculate the excess at that point. This is done with equation:

$$\text{excess} = N_{\mathrm{ON}} - N_{\mathrm{OFF}} \cdot \alpha. \tag{5}$$

α is the weighting factor for the background. It is needed since the data are analysed for several background positions. As FACT uses five background positions (see Figure 6) the weighting factor is 0.2.
The number of ON and OFF events can also be used to calculate the significance for each source position. This is done with the equation after Li, T. -P. and Ma, Y. -Q. 1983:

$$S = \sqrt{2}\left(N_{\mathrm{ON}} \ln\left[\frac{1+\alpha}{\alpha}\left(\frac{N_{\mathrm{ON}}}{N_{\mathrm{ON}}+N_{\mathrm{OFF}}}\right)\right] + N_{\mathrm{OFF}} \ln\left[(1+\alpha)\left(\frac{N_{\mathrm{OFF}}}{N_{\mathrm{ON}}+N_{\mathrm{OFF}}}\right)\right]\right)^{1/2} \tag{6}$$

The calculated excess and significance values for each source position are stored together with the corresponding position (Right Ascension and Declination) and the number of ON and OFF events.
Once the shell program has completed all the loops, and thus stored an excess and significance value for each position, these values are plotted. On the x-axis, Right Ascension and on the y-axis, Declination is plotted. The z-axis indicates in color the excess respectively the significance. The plots can be used to identify, if and where a source is visible.
Additionally a two-dimensional Gaussian

$$f(RA, DEC) = A \exp\left(-\left(\frac{(RA-RA_0)^2}{2\sigma^2} + \frac{(DEC-DEC_0)^2}{2\sigma^2}\right)\right) \tag{7}$$

is plotted as a γ-PSF on the excess data. The fit parameters are A as amplitude, RA_0 and DEC_0 specifying the centre of the peak and σ defining the width of the peak. The γ-PSF is fitted to the data, in such a way that 68 % of the signal is inside the circle with a radius of one σ.
If an extended source is to be identified, a γ-PSF of a point-like source is needed. Since even perfect point sources have a specific extension in the skymaps due to the detector and the analysis used, it is necessary to check how the skymap of a point-like source appears. If the γ-PSF of the possible extended source has a larger σ than the γ-PSF of the point-like source, it can be assumed that the source is extended and the extension can be derived. The γ-PSF depends also on the analysis. Different disp parameterizations can have an influence on the γ-PSF and therefore the angular resolution of the instrument.
The γ-PSF of the source Mrk421 is calculated and the results are discussed in the next section along with other results obtained from Mrk421 using the two-dimensional analysis.

4 Mrk421

The blazar Markarian 421 (Mrk421), subclassified as BL Lacertae (BL Lac) type object, is one of the nearest objects of the blazar class. The distance between Mrk421 and Earth is only about 400 million light-years (The American Association of Variable Star Observers n.d.). This makes Mrk421 easily observable for small telescopes like FACT. Furthermore, due to its blazar character, Mrk421 is variable in brightness, after Beck, M. et al. 2019. This makes it an interesting candidate for long-term observations to resolve this variability. It is therefore not surprising that Mrk421 is, with about 3400 hours, one of the most observed objects by FACT.
Because of this, and the fact that Mrk421 is a well-known point source in the gamma-ray regime, Mrk421 was used to test the code for the two-dimensional analysis. The results are shown in the following. In addition, the results are compared to plots from other telescopes, observing the gamma-ray regime, to confirm that they have a similar look.

4.1 Results

The code described in Section 3 was used to produce the Figures 11 to 14. The source was observed for about 17 h in the time between 16.01.2018 and 18.01.2018, leading to about 10 h of observation time after the data quality selection. The data quality selection was done with $R750_{Corr}/R750_{Ref}$ between 0.93 and 1.3 (Arbet-Engels, A. et al. 2021). The displayed area is $\pm 1.5^\circ$ in Declination and Right Ascension around the well-known source position. The source position at about Declination 38.2088° and Right Ascension 166.1140° is marked with a cross. Each square has the size of 0.1° times 0.1°.

4.1.1 Excess

The colour indicates the excess in Figure 11. The definition of excess can be found in equation 5. The source is clearly visible, as expected. This is the first indication of the functionality of the code.
Close to the source, some dark spots (negative excess) are visible. They also seem to have a symmetry and therefore do not seem to be random. One idea of where these spots come from is the analysis of the data taken in the Wobble mode, described in Section 1.3. Data taken in the Wobble mode are analysed for five OFF positions and the ON position, which explains the sixfold symmetry. Also part of the Wobble mode is the change of the pointing every 20 minutes. So in the data, there are two different positions of the source in the focal plane. This could explain why the symmetry is to the left as well as to the right of the

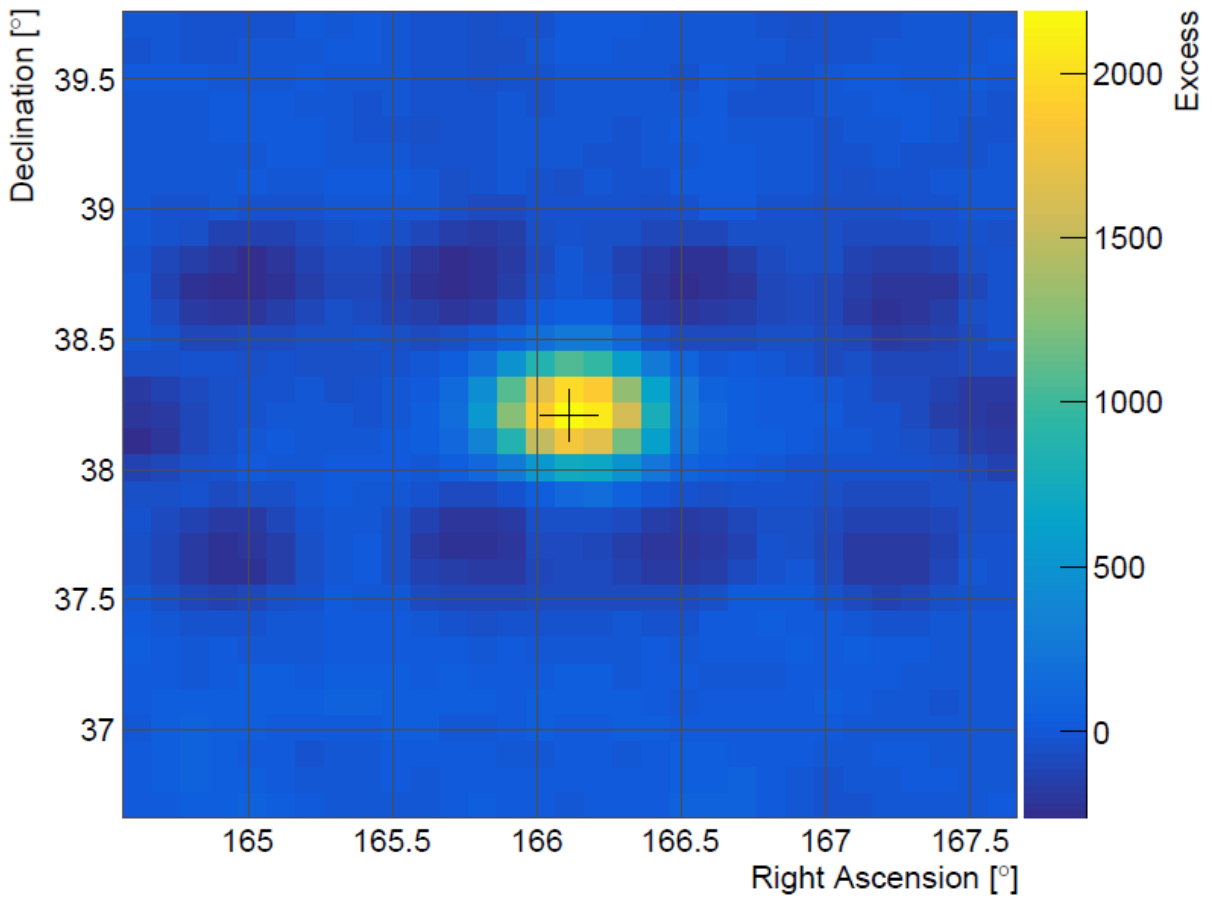

Figure 11: The excess plot for Mrk421 is visible. The plotted area is $\pm 1.5^\circ$ in Declination and Right Ascension around the source position, marked with a cross. Each square has a size of 0.1° times 0.1°. The colour indicates the number of events relative to the background.

source.

The point at which the analysis went wrong would then be the point at which the OFF focal plane positions are calculated. The OFF positions are calculated from the ON focal plane position by artificially rotating the ON position by a specific angle and calling it OFF. To visualize this one can look at Figure 6. The code described in this work changes the theoretical source position first. If the theoretical source position is now at the position of an nominal OFF position, as visible in Figure 6, the code would rotate one of the OFF positions into the nominal source position (ON in Figure 6). The source is well visible with a high number of events at the nominal position, leading to a high number of background events for this new theoretical source position. This could explain the negative excess, as

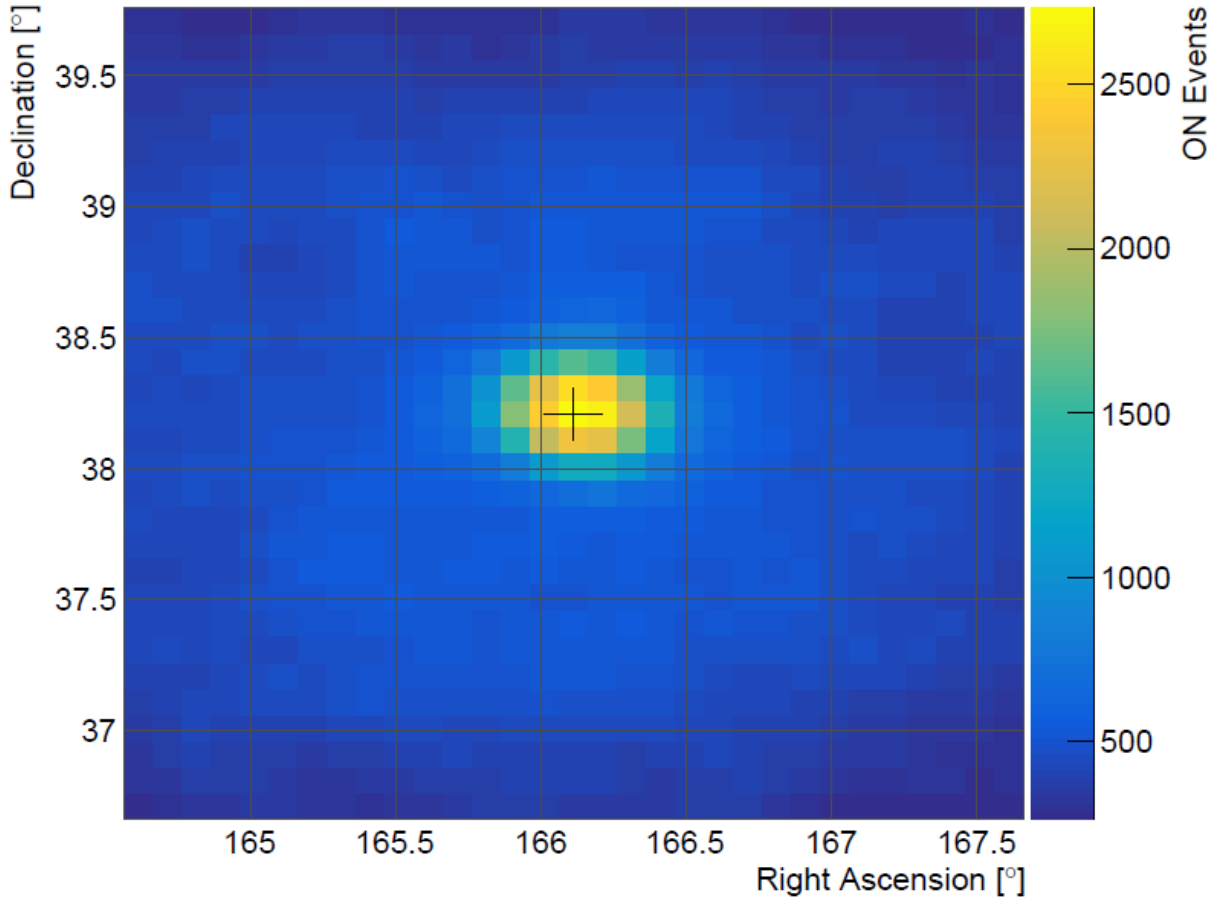

Figure 12: The ON events for each position are plotted. The plotted area is $\pm 1.5^\circ$ in Declination and Right Ascension around the source position of Mrk421, marked with a cross. Each square has a size of 0.1° times 0.1°. The colour indicates the number of ON events.

for negative values the number of OFF events must be five times greater than the number of ON events.

4.1.2 ON and OFF

To better see where the dark spots come from, the excess plot is split into two plots, one with only the ON events (Figure 12) and one with only the OFF events (Figure 13). In the skymap with only the ON events, the source Mrk421 is visible and there are no dark spots. So it seems that the ON data are not causing the symmetrical spots in the excess plot.

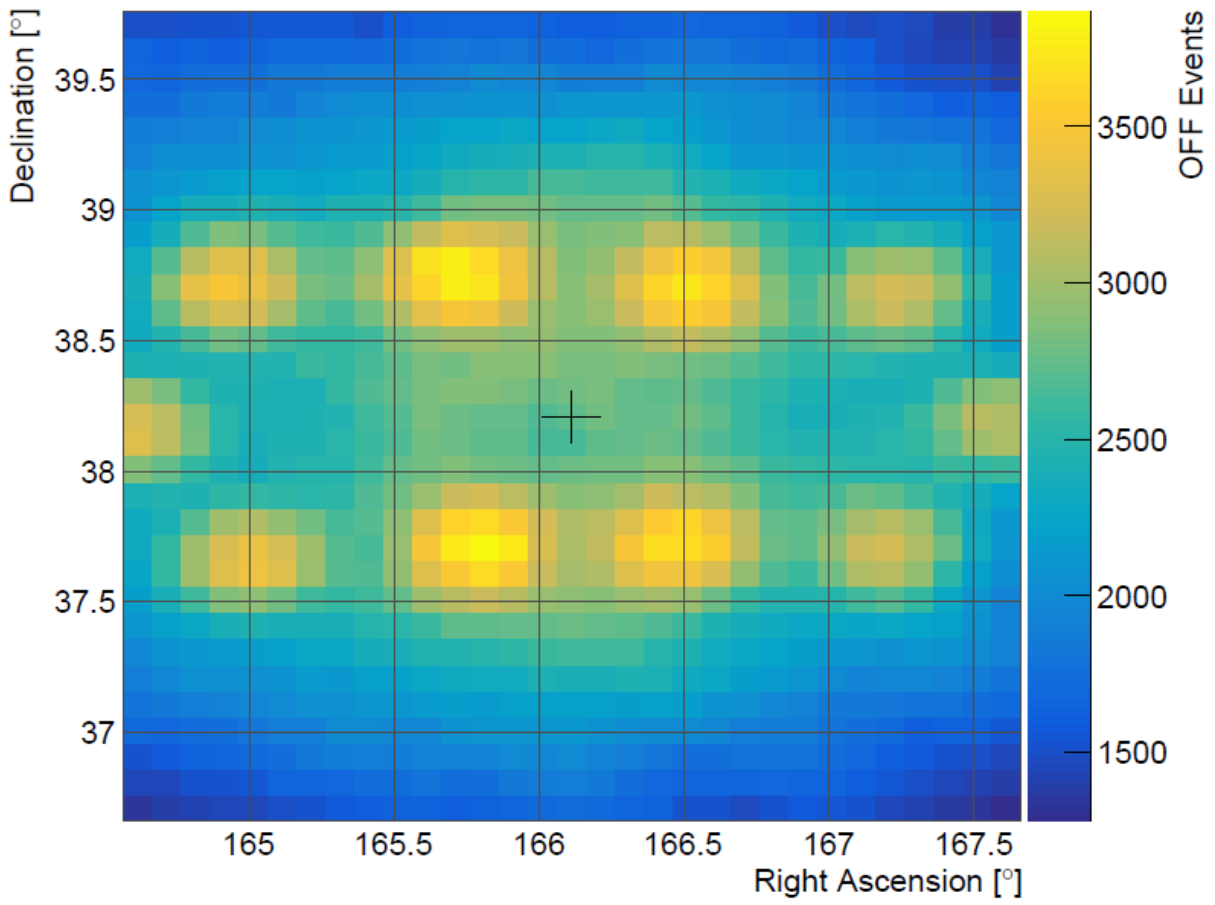

Figure 13: The OFF events for each position are plotted. The plotted area is $\pm 1.5°$ in Declination and Right Ascension around the source position of Mrk421, marked with a cross. Each square has a size of $0.1°$ times $0.1°$. The color indicates the number of OFF events.

However, in the OFF skymap, there are bright spots corresponding to the dark spots in the excess plot. The symmetry is not directly visible as the bright spot of the source Mrk421 in the centre is missing. This is because the bright spot of Mrk421 consists of ON events and is therefore not expected to be visible in the OFF data.
The fact that the symmetrical spots are only visible in the OFF data supports the theory explained in the last section. This theory states that the bright spots in the OFF map are remnants of the signal data of Mrk421 when the ON position is chosen to be at the same position as one of the nominal OFF positions. This would result in one of the current OFF positions being in the same position as the nominal ON position, with the signal data from Mrk421 now being used as background.

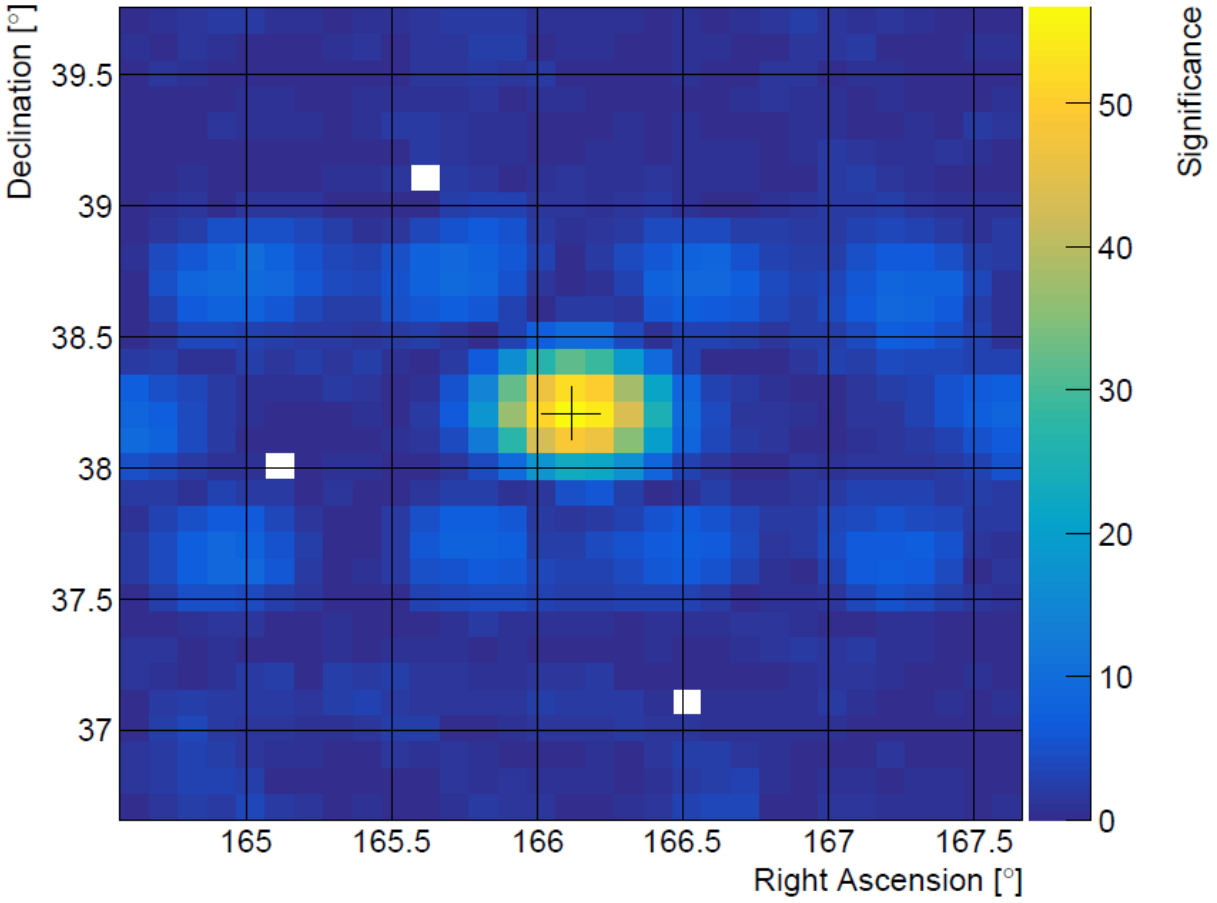

Figure 14: The significance map for Mrk421 is visible. The plotted area is $\pm 1^\circ$ in Declination and Right Ascension around the source position, marked with a cross. Each square has a size of 0.1° times 0.1°. The colour indicates the significance at that point. For the three white squares, the algorithm failed to calculate the significance.

This is one of the aspects that need to be improved or solved in the future. This will be discussed further in Section 6. Although these spots are visible in the skymap, the source is clearly identifiable, as already shown in Figure 11. This is also the case for the significance plot discussed in the next section.

4.1.3 Significance

In addition to the excess map also a significance map can be calculated from the number of ON and OFF events. This map is shown in Figure 14, the color indicates the significance. The definition for the significance can be found in equation 6 in Section 3.4. Again, the source is clearly visible and looks similar to Figure 11. This makes sense as the significance

is calculated using the number of ON and OFF events. The main visible difference to the excess plot is the colour of the systematic pattern.
What is noticeable is that the spots have a positive value, whereas they were negative in Figure 11. This can be explained by the calculation of the significance. Looking at equation 6, it can be seen that the number of ON and OFF events are only added up and multiplied, which only leads to positive significance.
In the skymap, also three white squares are visible. This is due to the algorithm used to calculate the significance. As can be seen in equation 6, the inner part of both natural logarithms gets 1, if the number of OFF events is exactly five times the number of ON events. Since $\ln 1 = 0$ is valid, the algorithm fails. No significance could be calculated for these squares, so they are left blank. To verify this, the values of these squares are checked in the excess plot (Figure 11). It is observable that these points have an excess of exactly zero, as expected.

4.2 Discussion

To further examine the plots of Mrk421 and therefore also the code, the significance plot is compared with a plot made using data from the HAWC telescope. Furthermore, a two-dimensional Gaussian is plotted to the data to see the size of a point source in the FACT telescope. This is an indication of whether the analysis of the data needs to be improved. Additionally, it can be used as a reference size to compare with possible extended sources.

4.2.1 Comparison to HAWC Data

The **H**igh **A**ltitude **W**ater **C**herenkov gamma-ray observatory (HAWC) is a water Cherenkov telescope consisting of 300 water tanks located at 4100 m a.s.l. in Mexico. It has a field of view of $\sim 2\,\mathrm{sr}$ (steradian). The plot used for comparison consists of data taken during 1038 days of exposure. In addition, only gamma photons with reconstructed energies above $0.5\,\mathrm{TeV}$ are taken into account in the plot. The data were collected between June 2015 and July 2018. This is explained in Albert, A. et al. 2022.
The skymap by HAWC is shown in Figure 15. It is important to note that this skymap is mirrored on the y-axis compared to the skymaps in Section 4.1. This means that the values on the x-axis become smaller the further on the right ones get. This has to be taken into account when comparing the two significance maps.
First of all, it is visible that the resolution is slightly better than in the plots shown in Section 4.1. One reason for this is the lack of time, as the production of a plot with the

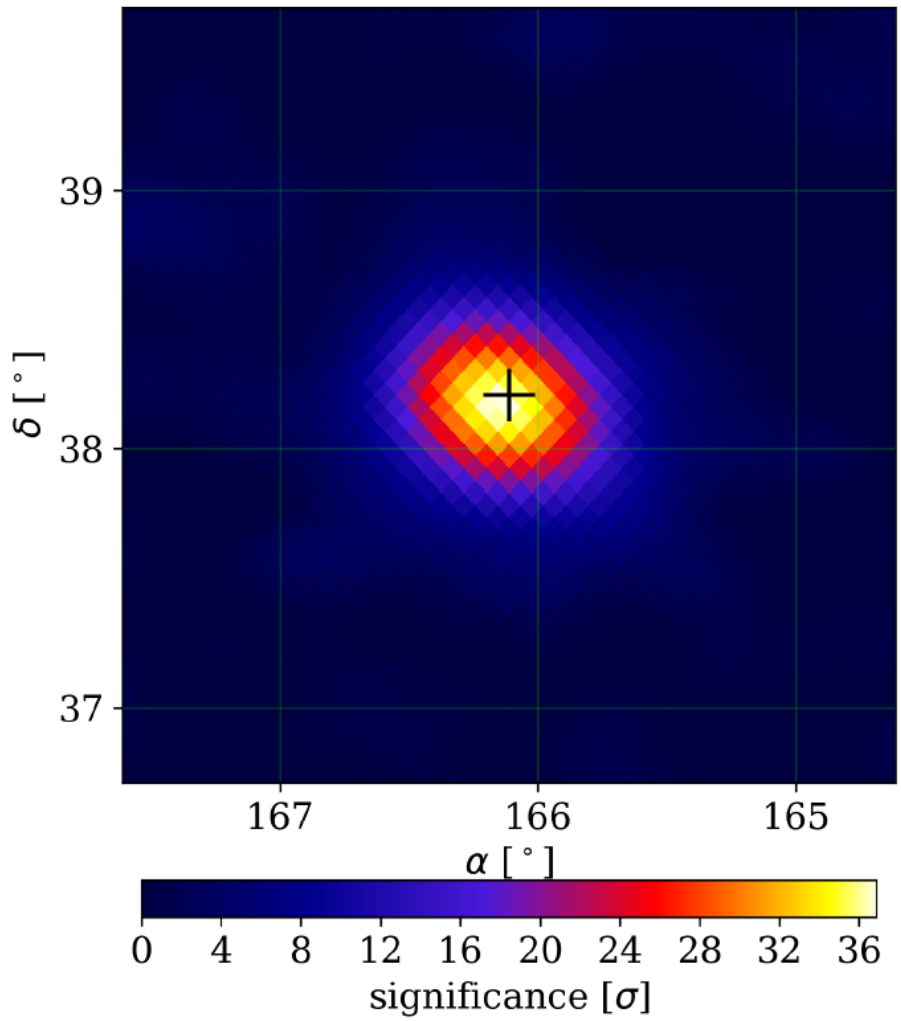

Figure 15: A significance plot with data from the HAWC telescope is shown. The colour indicates the significance of each point. The Figure is taken from Albert, A. et al. 2022.

current code takes a long time. Another reason is that even with a better resolution nothing new is expected to be observed. Nevertheless, in Figure 14 and Figure 15, the source Mrk421 is well visible. In both skymaps, the source also seems to be at the same position, when taking into account that the x-axis is defined differently. This confirms the general functionality of the program.

The main difference between the two Figures 14 and 15 is that the significance map with the data from HAWC has no systematic spots. There are some randomly distributed brighter parts in the skymap but this is to be expected as the background is statistically. This is good evidence that the spots visible in Figure 14 cannot be random uncertainties in the data, but are artefacts of the analysis code. Otherwise, the spots should also be visible in

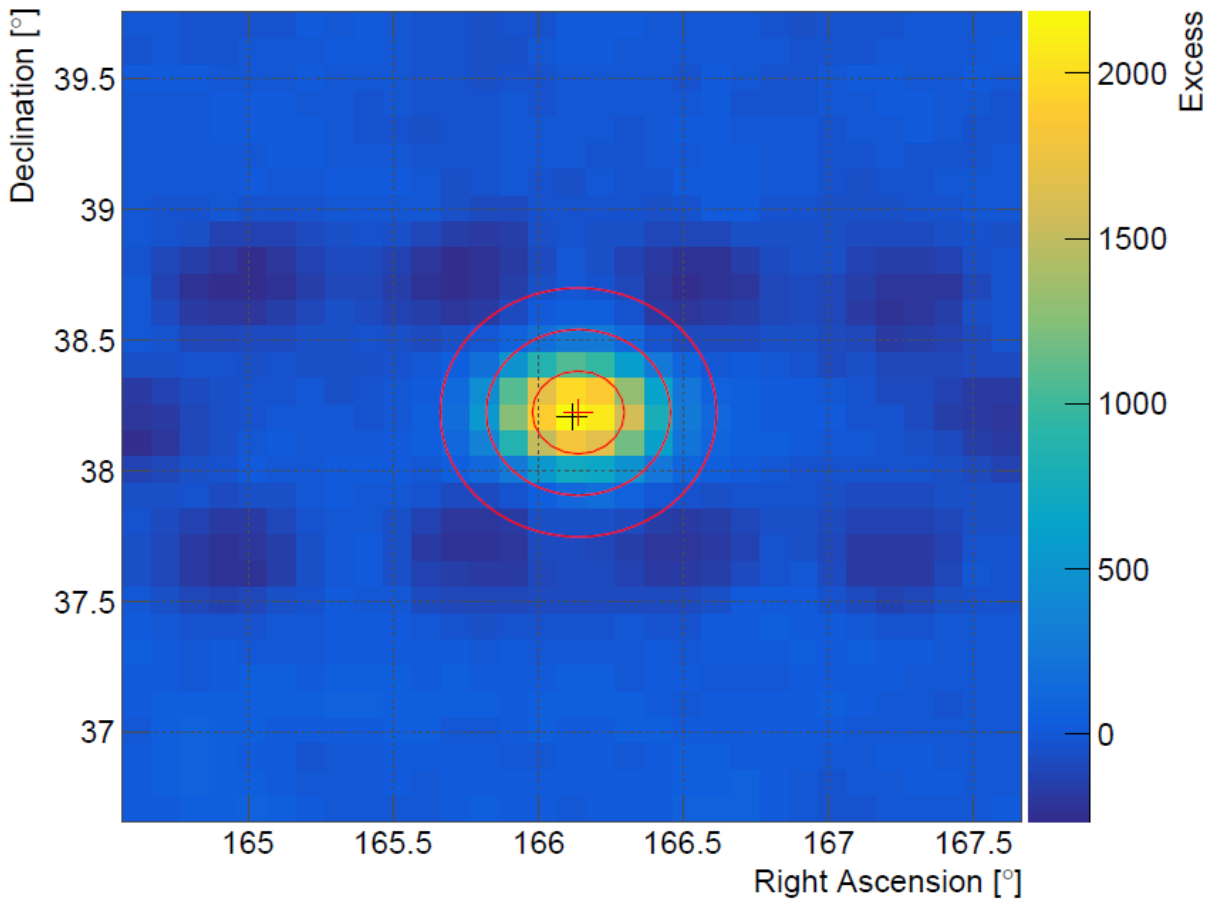

Figure 16: The same plot as in Figure 11is visible, but additionally, the one, two and three sigma values of a two-dimensional Gaussian fit of the data are shown as red circles. The source position calculated by the fit is marked with a red cross. The black cross indicates the nominal source position of Mrk421.

Figure 15.

4.2.2 γ-Point Spread Function

A point-like source also has a specific extension in the skymaps due to the detector and the analysis. To specify this extension, a γ-PSF can be fitted to the data of a point-like source, like Mrk421. This defined γ-PSF can then be used to identify extended sources. To do so, the size of the γ-PSF is compared to the extension of the possibly extended source. If the size of the possibly extended source is larger than the size of the γ-PSF it can be assumed that the source is indeed extended. To determine the γ-PSF, the extension of Mrk421 in the skymap is identified.

variable	fitted value
A	2432 ± 41
RA_0	$(166.1360 \pm 0.0030)^\circ$
DEC_0	$(38.2238 \pm 0.0026)^\circ$
σ	$(0.1588 \pm 0.0018)^\circ$

Table 2: Displayed are the parameters of a two-dimensional Gaussian (equation 7) fitted to the data of Mrk421. The received values are shown with errors.

fit parameters	values
Chi2	$6.76372 \cdot 10^6$
Ndf	957
Edm	$4.38215 \cdot 10^{-7}$
NCalls	128

Table 3: The fit parameters, which specify the calculation of the fit, are displayed. The values for ChiSquare (Chi2), the number of degrees of freedom (Ndf), the expected distance to the maximum (Edm) and the number of function calls (NCalls) are given.

The Mrk421 data are fitted with equation 7. The fit results and fit quality values are reported in Table 2 and Table 3. The number of degrees of freedom (Ndf) seems reasonable if one considers the number of data points. The expected distance to the maximum (Edm) and the number of calls of the fit function (NCalls) are small, indicating a good and fast fit to the data. The χ^2 value (Chi2), however, is relatively large, speaking against well-fitted data. This was further investigated by plotting the counted events in dependency of Right Ascension respectively Declination, for a fixed value of DEC 38.2088 ° and RA 166.114 °. In addition, the corresponding two-dimensional Gaussian fit is added. The Figures 22 and 23 can be found in the appendix. If one compares the histogram and the Gaussian fit, in both Figures, no discrepancies, which could explain the high χ^2 value, are visible.
All the fit results are in the right order of magnitude if one compares them to the data. The errors of these are small indicating also a good fit. Furthermore, the fitted values for the source position, the centre of the peak (RA_0 and DEC_0), is very close to the nominal position of Mrk421. But due to the small errors they only match at about 7.4 (RA) respectively 5.8 (DEC) times the error, when considering the database values as error-free. The value σ, the width of the peak, also seems to make sense because of the small error.
The centre of the peak is also visible in Figure 16, marked with a red cross. In comparison,

the black cross is still visible as the position of the source given by the database. In Figure 16, the excess data already shown in Figure 11 and discussed in Section 4.1.1 are displayed. Additionally circles with radii of one, two and three σ around the peak centre are added to the skymap.
With that, the width of the fit can be compared to the width of the source visible in the skymap. It appears that the one σ circle already contains the brightest parts of the source. Almost all of the excess of the source is within the two σ circle. This is consistent with the definition that about 95 % of the signal should be within the two σ area.
However, looking at the value of σ and comparing it to the values of other telescopes, it is noticeable that the radius of the γ-PSF of FACT is larger than that of the other telescopes. For example, the angular resolution of MAGIC according to Aleksić, J. et al. 2016 is in the range of 0.035 ° to 0.09 ° depending on the energy of the primary particle. And the σ value for the HESS telescope according to Cornils, R. et al. 2003, is 0.33 mrad or 0.32 mrad depending on the telescope. This is about 0.0185 °. Both telescopes therefore have a smaller γ-PSF, resulting in better resolution compared to FACT. One thing that may explain this, at least in part, is that MAGIC and HESS consist of several individual telescopes which are operated jointly. The cooperative observation improves the angular resolution.
The γ-PSF depends on both the telescope itself and the analysis of the data. To improve the resolution of FACT and therefore the γ-PSF, the analysis of the data needs to be optimised.
The γ-PSF obtained with Mrk421 can be used to identify extended sources. But it would still be interesting to determine the γ-PSFs of other point-like sources, like the Crab Nebula, to see if differences are detected.

5 The Galactic Centre

The galactic center is the central region in our galaxy, the Milky Way. In its centre, a supermassive black hole, Sagittarius A*, with around 4 million solar masses, exists. Besides the supermassive black hole, many other objects are located near the galactic centre, making the sky region very crowded. This together with the small FoV of FACT makes the region of the galactic centre difficult to analyse. Due to the high number of observable objects, they can interfere with each other. This makes the detection of individual objects complicated. This information was taken from Evans, J. and Friedlander, M. W. 2024.

5.1 Results

The code is used to calculate the data from the galactic centre plotted in Figures 17 to 20. The source was observed for about 52 h in the time between 20.06.2014 and 22.08.2014. This leads to about 33 h after the data quality selection, which was done using $R750_{Corr}/R750_{Ref}$ between 0.93 and 1.3 (Arbet-Engels, A. et al. 2021). The resulting skymaps are shown in Figures 17 and 18. The Figures 19 and 20 contain only about 2 h of data (after the data quality selection) observed between the 17.07.2014 and the 19.07.2014. The position of the galactic centre is at Right Ascension 266.5 ° and Declination −29.01 °. Each square has the size of 0.1 ° times 0.1 °.

5.1.1 Full Data Sample

Because Figure 17 is produced with around 33 h of data, the displayed area is rather small. The area is ± 0.5 ° around the position of the galactic center, marked with the black cross. In this plot, the colour indicates the excess. The source is not visible at the nominal position. At a larger Declination value, the excess rises and could indicate a source. So the source may be detected at a different position.
To confirm this also the significance plot needs to be investigated. The skymap (Figure 18) shows a higher significance at the same position. So this also confirms the indication of a source. But one can only declare the detection of the source when the significance for that position exceeds 5 σ. As this limit is not met, with the highest significance being 4.67 σ, by the area in the skymap, the source was not detected. More data are needed to get from an indication of a source to a detection. This is discussed further in Section 5.2.1.
Another higher significance is visible in Figure 18 in the lower left corner, but this is due to high negative excess caused by high background values. This can be seen in Figures 24 and 25 in the appendix. These are the skymaps with only the number of ON or OFF

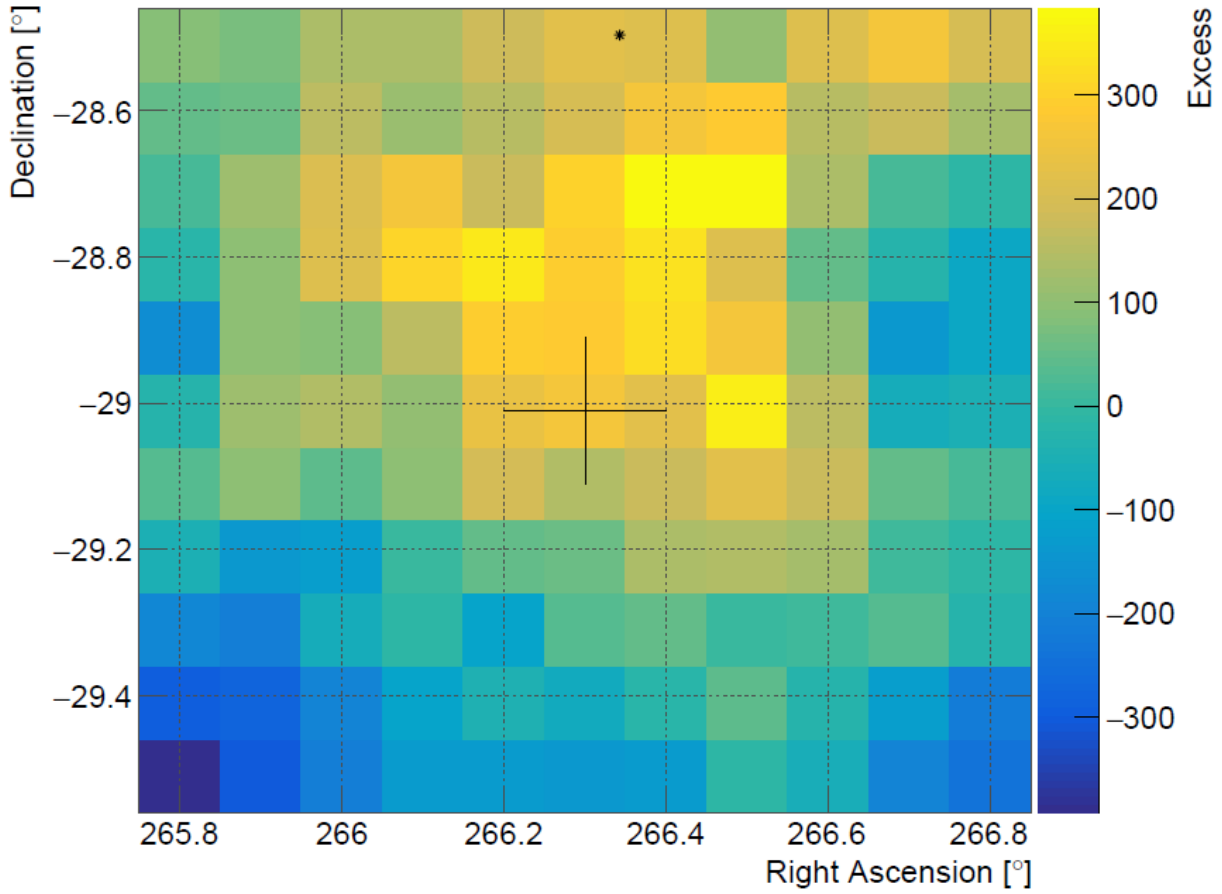

Figure 17: The area $\pm 0.5^\circ$ in RA and DEC around the galactic centre is shown. For this skymap, about 33 h of data (after data quality selection) are used. The colour indicates the excess. Some excess near the position of the galactic center is visible. The stars mark objects having a magnitude brighter than 9 in the B-band. The data for this object are received from the SIMBAD database.

events.

Additionally, a position in Figure 17 is marked with a black star, representing an object having a magnitude brighter than 9 in the B-band. This is the magnitude in the optical blue part of the electromagnetic spectrum. The position of this object is added to this skymap, as bright objects in the FoV of FACT lead to a higher night sky background. This leads to more noise and therefore the signal extraction gets more difficult. In addition, due to different analytical responses, inhomogeneities in the night sky background can lead to fluctuations in the sky map. This is further discussed in Section 5.2.2.

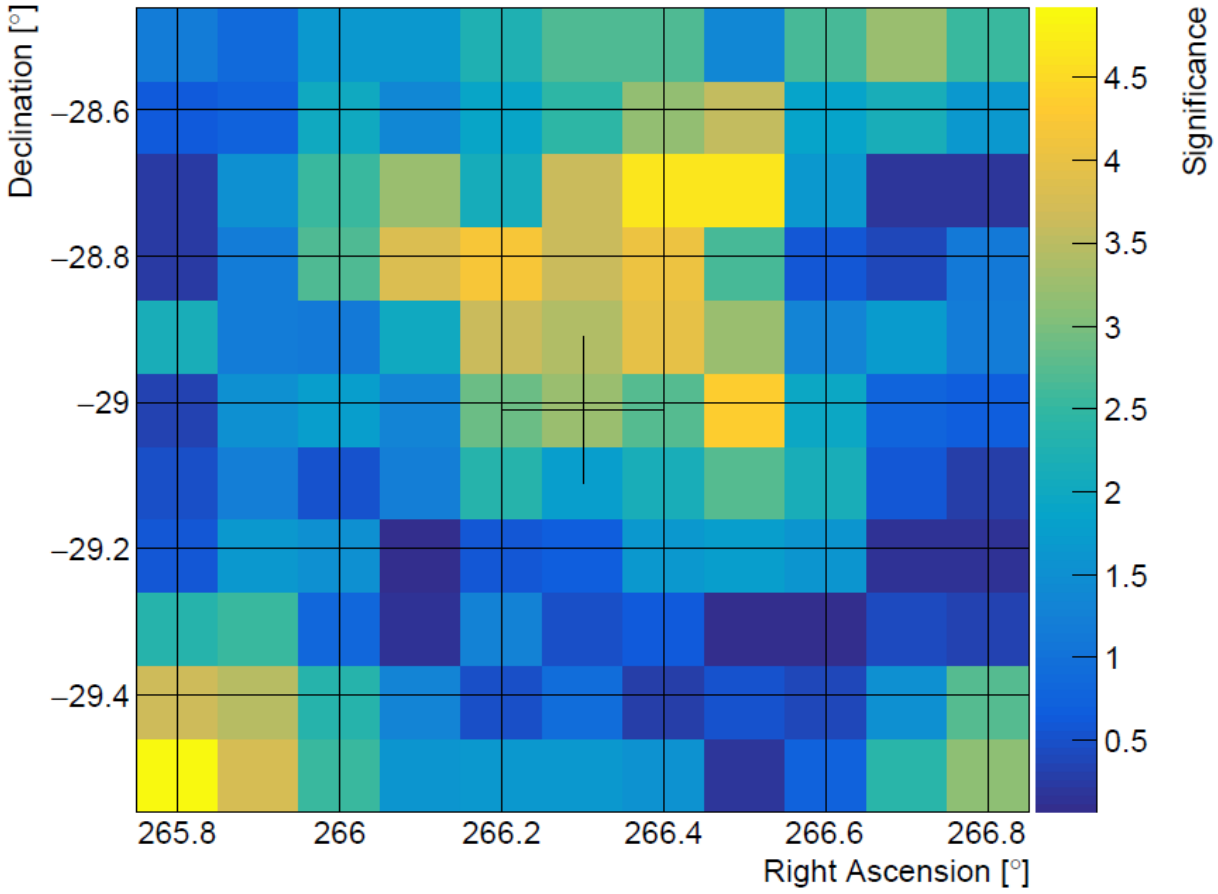

Figure 18: An area of $\pm 0.5^\circ$ in RA and DEC around the galactic centre is shown. The skymap consists of around 33 h of data, after data quality selection, taken in around two months. The colour indicates the significance. For two areas the significance is slightly higher.

5.1.2 Partial Data Sample

Besides analyzing all the data at once for a small area around the nominal source position, the data of only three nights, meaning 2 h after data quality selection, are analyzed. This is done for an area of $\pm 1.5^\circ$ in Right Ascension and Declination around the nominal source position. In Figure 19, the results are displayed. The colour indicates the excess. The excess is not high at a specific position, but also no large negative values are visible. Nevertheless, some sort of pattern is visible. The lower left part has a mainly negative excess and the upper right part is mainly positive.
Additionally, objects with a B magnitude smaller than 9 are plotted onto the excess plot. The stars represent the positions of the objects. The objects seem to be randomly dis-

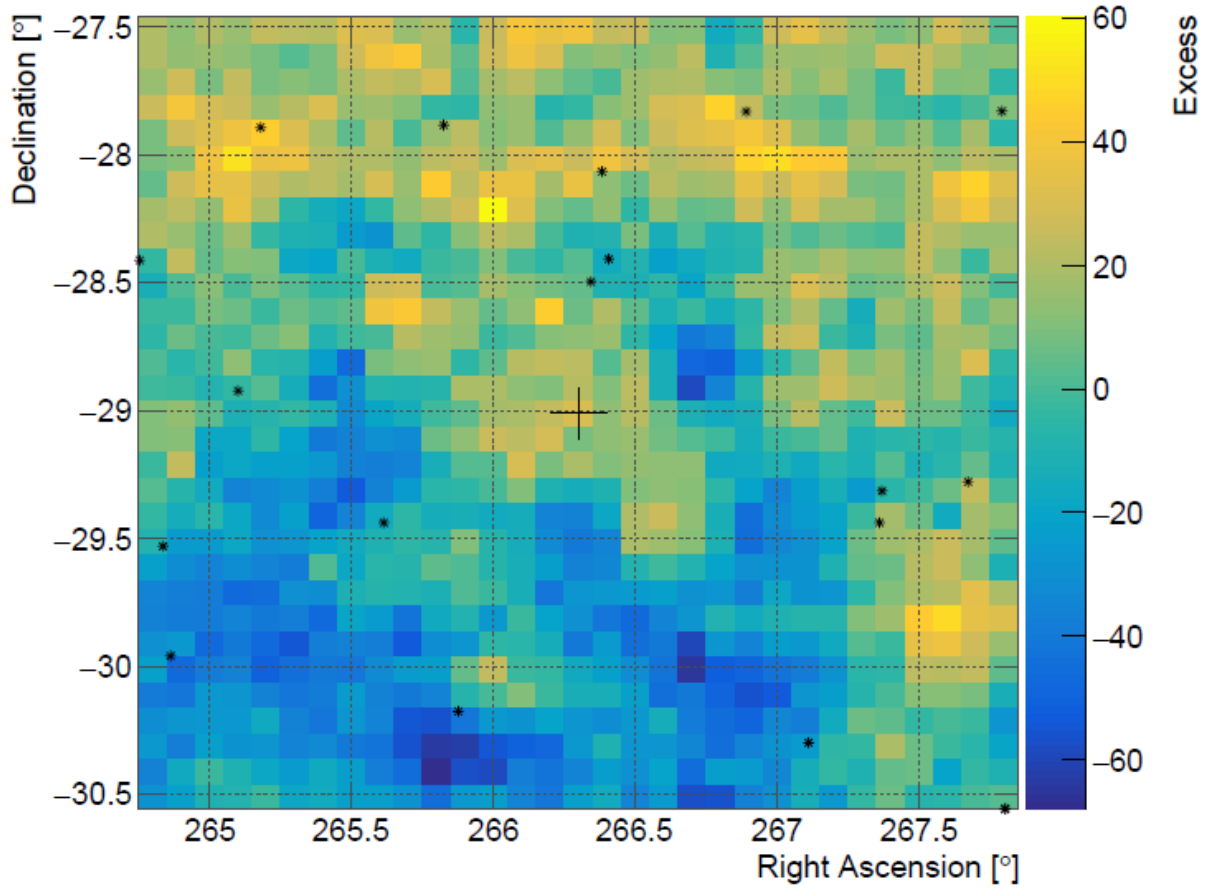

Figure 19: The area ($\pm 1.5^\circ$ in RA and DEC) around the galactic centre is visible. The position of the galactic center is marked with a cross. The colour indicates the excess for each position. 2 h of data are analyzed for this skymap. No source seems to be detected. The stars represent objects with a magnitude higher than 9 in the B-band. The information about the objects is from the SIMBAD database.

tributed. If some sort of pattern would be visible in the distribution of the objects, the excess could be compared to it. This is further discussed in Section 5.2.2.
To further investigate the pattern in the excess plot, the number of ON and OFF events are plotted separately. The number of ON events for each position is shown in Figure 20. In this skymap, a bright extended area is visible. It is not expected that the galactic centre has such a huge extension. However, it is possible that other sources, emitting in the gamma-ray regime, are near the galactic centre and disturbing the measurement of the galactic centre. This is further discussed in 5.2.3.
The same is visible for the OFF events in Figure 26 in the appendix. Here, also a bright,

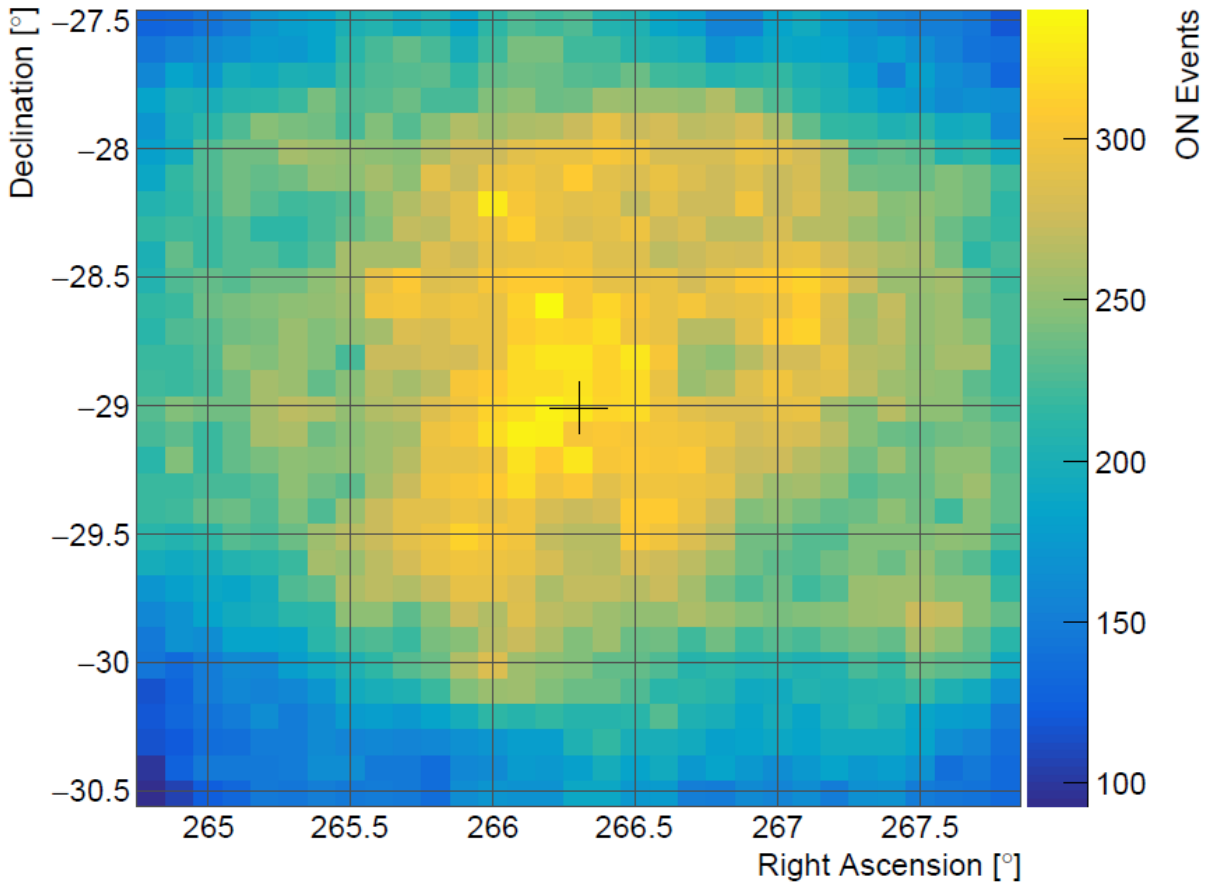

Figure 20: The area with $\pm 1.5\,^\circ$ in RA and DEC around the galactic centre, marked with a cross, is shown. The colour indicates the number of ON events. 2 h of data are analyzed for this skymap. A large defuse higher number of events is visible around the galactic center.

even bigger, extended area is visible. This can be explained with the five OFF positions (described in Section 1.3) that are used to describe the background at each position. The several background positions lead to the smearing of the OFF data. This could explain the larger area compared to the ON data.

In the significance plot (Figure 27) in the appendix, no high significance values, corresponding to any source, are visible. The only higher values, in the bottom left corner, correspond to negative excess due to a huge number of background values. This large number of background events is visible in Figure 26 in the appendix.

5.2 Discussion

To further discuss what is visible in the skymaps of the galactic centre, the nearby objects need to be examined. Both objects emitting in the optical blue regime and objects emitting in the gamma-ray regime need to be considered. Before doing this, it needs to be checked whether a detection of the galactic centre with FACT is feasible in the given exposure.

5.2.1 Observation Time of the Galactic Centre

If a source can be detected by a telescope, is among others dependent on the time the telescope observed the source and on the brightness of the source. The brighter the source, the less observation time is needed. After Bretz, T. et al. 2012, FACT has a sensitivity of 8 % of the Crab Nebula in 50 h. This means that FACT can detect a source with a brightness of 0.08 **C**rab **U**nits (CU) if the source was observed for 50 h.
After Adams, C. B. et al. 2021, the galactic centre has a flux of about 0.1 CU for an energy above 1 TeV. With this the needed observation time can be calculated by solving

$$\frac{0.1}{0.08} = \frac{\sqrt{50\,h}}{\sqrt{x\,h}} \tag{8}$$

for x. This leads to an observation time of around 32 h. FACT has observed the galactic centre for about 52 h, which leads to about 33 h of data after the data quality selection. This is just enough to detect the galactic centre. However, this is only a rough estimate, as only energies above 1 TeV have been considered, but FACT also observes at lower energies. This difference in the part of the spectrum considered affects the flux. The spectral index of the galactic centre is 2.12 (after Adams, C. B. et al. 2021) and of the crab nebula 2.5 (after Abdo, A. A. et al. 2012). For both the exponential cutoff power law model is assumed. The spectral index of the crab nebula is higher, leading to a higher integrated flux compared to the galactic centre. The difference becomes even larger when lower energies are considered. This leads to a lower brightness of the galactic centre in Crab units if energies below 1 TeV are also considered. As this could be taken into account for FACT, the required observing time increases.
This can explain why the significance in Figure 18 is not high enough for the detection of the source. By observing the galactic centre again and taking more data, the significance can be increased until the source can be detected.
This could also explain why nothing is visible in the excess map (Figure 19). As with only 2 h of data and a brightness of 0.1 CU it is very unlikely to detect the source in the data. Besides the additional needed observation time, all the data should be analyzed for a larger

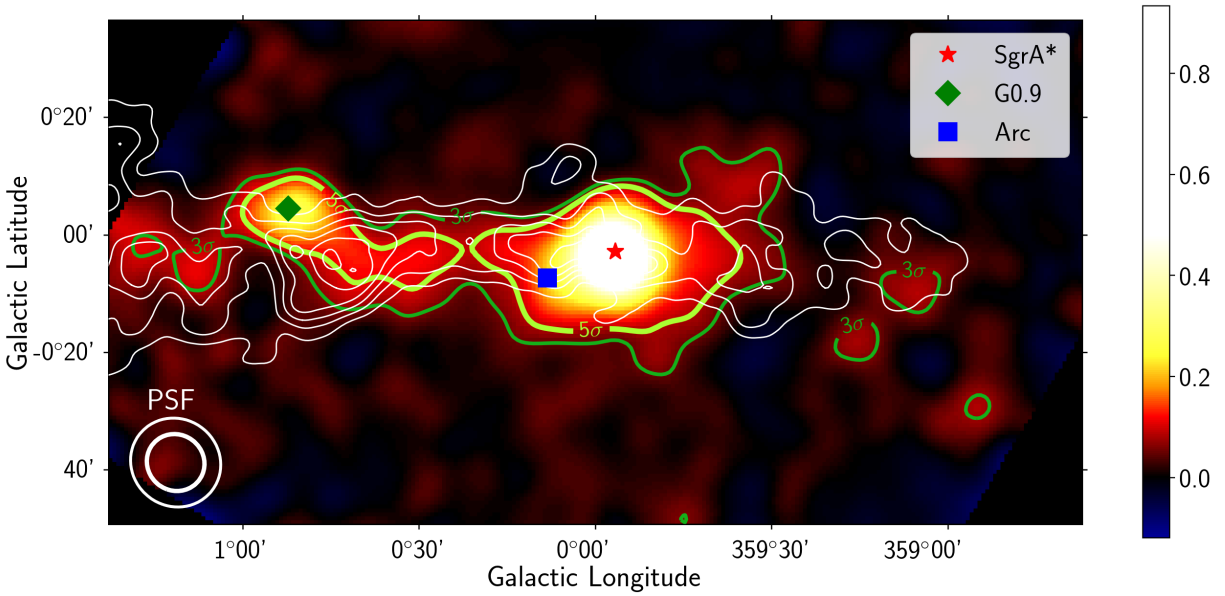

Figure 21: The area around the galactic centre in gamma rays is shown. The data were taken by the MAGIC telescope. Three sources, each of them marked with a symbol, are visible in that region. The colour indicates the fraction of excess over the background. The green line represents the $5\,\sigma$ and $3\,\sigma$ markings. The γ-PSF of MAGIC is also given in the lower left corner. The two circles represent the 39 % respectively 68 % containment contour. The Figure was taken from MAGIC Collaboration and Acciari, V. A. et al. 2020.

area in the sky. This can help to clearly identify the position of the source, as it seems that the significance is slightly shifted compared to the coordinates given in the database. The larger sky area could also help to identify other nearby sources, as they can complicate the analysis of the galactic centre region. The interference would also increase with increasing observation time due to the higher significance of all sources.

5.2.2 Nearby Objects Emitting in the Optical Blue Regime

The optical blue regime needs to be taken into account due to the Cherenkov photons (described in Section 1.1.2) also being mainly in the optical blue regime. So when there are objects in the FoV of FACT, the night sky background is increased. This leads to more noise in the signal. With this, less signal can be extracted, as fewer pixels survive the image cleaning. Effects of this can be visible in the skymaps if the distribution of these sources is not homogeneous, as this would lead to an inhomogeneous night sky background.
As already described in Section 5.1, the stars visible in Figure 17 and 19 represent objects having a magnitude brighter than 9 in the B-band.

After[9], the B magnitude describes the magnitude in the optical blue regime when using the Johnson photometry system. The wavelength of the filter is centered at 436 nm and the bandwidth is 89 nm.
The close objects seem to be randomly distributed. In addition, the objects in Figure 19 do not seem to correspond to specific increases in the excess. One difficulty with these skymaps is the short observation time, which results in a low gamma-ray statistic. This may explain the failure to detect variations in the night sky background caused by the discussed objects.
In Figure 17, only one bright B magnitude object is visible. For this object, no corresponding fluctuation in the night sky background can be identified. To confirm this, more data and a larger area are needed due to the reasons already explained in Section 5.2.1.
As the pattern visible in Figure 19 can not be explained with the objects displayed in this section, also fainter objects should be taken into account, as they can still influence the night sky background. This can be seen in Figure 28 in the appendix, for a magnitude higher than 30 in the B-band. But also these objects seem to be distributed randomly and therefore do not correspond to any observed fluctuations in the skymaps.

5.2.3 Nearby Objects Emitting in the Gamma-Ray Regime

Furthermore, gamma-ray sources near the galactic centre must be taken into account. This can be done with Figure 21. The data are from the MAGIC telescope. In this skymap, the galactic centre, here SgrA* (the supermassive black hole in the centre of the Milky Way), is marked with a red star. Additionally, two more sources are marked in this skymap. It needs to be mentioned, that the coordinate system, in the MAGIC paper, is different compared to all other skymaps in this bachelor thesis. So only the distances can be compared easily. The colour represents the fraction of excess over the background. This represents how much the excess exceeds the background value. The green lines show the $5\,\sigma$ and $3\,\sigma$ confinements. In the lower-left corner, the γ-PSF of MAGIC is shown.
It is visible that in the vicinity of $1\,^\circ$ two additional objects are located. The object Arc is so close to the galactic centre that the two sources cannot be separated. To see if the excess and also the significance visible in Figure 17 and 18 is caused by Arc and not by the galactic centre, the coordinates for this source must be transformed into ICRS. This is done with astropy. With a position of $0\,^\circ 15'$ in longitude and $-0\,^\circ 05'$ in latitude, the result is about $266.56\,^\circ$ in Right Ascension and $-28.87\,^\circ$ in Declination.
If this is now compared to Figure 17 it is visible that the position of higher excess fits very

[9] https://www.oxfordreference.com/display/10.1093/oi/authority.20110803095514180

well to the position of Arc. After MAGIC Collaboration and Acciari, V. A. et al. 2020, the flux of Arc is about $6 \cdot 10^{-14} \frac{ph}{cm^2 sec}$ and therefore much weaker than the flux of the galactic centre, with about $35 \cdot 10^{-14} \frac{ph}{cm^2 sec}$, making it unlikely that FACT indicates the object Arc. For both the energy threshold is 1.2 TeV. Again to investigate this further, more data are needed and the full set of data must be analyzed for a larger area in the sky.
In total, one can say that more data are needed to confirm the detection of the galactic centre or any other source in the gamma-ray regime. The full set of data should be analyzed for a larger area in the sky, to be able to compare the signal with the background. With that, the detection of the galactic centre or other nearby sources can be confirmed in the future.

6 Summary and Outlook

In this work, the program for a two-dimensional analysis of FACT data was introduced. Two sources were analysed with the program to test if the developed code works.
The first source is Mrk421, a well-studied point-like source. This makes Mrk421 the perfect source to test the functionality of the program. The results demonstrate that the program is working, as the source Mrk421 is visible in the skymaps. However, all positions are analysed equally without considering additional information on the location of known sources, producing artefacts in the skymaps. This is because some of the positions used by the program in the background estimation happen to be at the position of the source, in this case, Mrk421. This leads to a high number of background events for certain positions, causing the visible systematic pattern. To solve this problem, the known sources have to be excluded from the background estimation. One possibility is to define the size and value of the artefacts, by fitting a Gaussian function to them and subtracting the fit again from the data.
Additionally, the γ-point spread function is determined from the data. This is done to see what a point source looks like in the FACT analysis. The γ-PSF can then be used to identify extended sources by comparing their sizes. Fitting a Gaussian distribution to the skymap of the point-like gamma-ray source Mrk421 yields a γ-PSF of $(0.1588 \pm 0.0018)^\circ$. Comparing this to the values of other telescopes, the value seems large. To minimize the γ-PSF of FACT, the analysis needs to be optimized. Additionally, other point-like sources should be analysed to crosscheck the results for the γ-PSF with those data.

The other source discussed in this work is the galactic centre. It is interesting to analyse the galactic centre with the two-dimensional analysis, as the area around the galactic centre is very crowded with other sources. A small area around the galactic centre is analysed for the about 33 h of data (after data quality selection). These skymaps may indicate a source, but more data are needed to confirm the detection of a source.
Furthermore, the increase found in the excess map is not at the nominal position of the galactic centre. To investigate this further, information from the MAGIC telescope about other sources near the galactic centre emitting in the gamma-ray regime are taken into account. Another object that would fit the position of the increased excess is the object Arc. However, due to the fainter brightness, it is unlikely that this object is the cause of the increased excess. To confirm this more data are needed.
As FACT has a sensitivity of 8 % of the Crab Nebula in 50 h of observation (Bretz, T. et al. 2012), the calculated observation time needed is about 32 h. This amount of time was

observed, but the source could only be indicated. As this can be seen as a lower limit for the observation time further observations of the galactic centre should lead to a detection. In addition, it can be helpful to plot a larger area around the galactic centre to reveal other sources and have a larger background area. This was tried with 2 h of data after the data quality selection. However, due to the low brightness of the galactic centre, no source is visible in these skymaps. Yet the distribution of the excess does not seem to be completely random. To test if this distribution can be explained by objects emitting in the optical blue regime, these objects with a B magnitude smaller than 9 are plotted on top of the excess skymap. No correlation can be identified.

In total, one can say that more data of the galactic centre are needed. These data must then be analysed for a larger area in the sky. In future, this can lead to a detection of the galactic centre or other sources nearby.

To be able to do all this and to analyse more sources efficiently, the program described in this work will be optimised in the future. This leads to a faster analysis of the data and makes it possible to find new interesting objects in the sky. The program can then be used to search for unidentified sources in the data as an area around the observed position can be analysed. In addition, the analysis can be applied to data taken during follow-up observations of alerts from neutrinos or gamma-ray hotspots, which often have a large uncertainty of the position.

Acknowledgment

I would like to thank Prof Dr Karl Mannheim for giving me the opportunity to write this bachelor thesis. I would also like to thank Dr Daniela Dorner for her excellent support with questions and other problems. I also appreciate her great help with proofreading. I wish to thank the whole Mannheim group for the warm welcome in the group and for the help with minor and major problems. In particular, I would like to thank Marcel, with whom I had many stimulating discussions. In Addition, I wanted to thank Julia, with whom I had many interesting discussions and who sometimes showed me a new perspective. Of course, I am grateful to my family, who have always supported me along the way. They have always given me the strength to carry on. I am thankful to my friend Kaeil, who often had to take a back seat but always stood by me.

7 Appendix

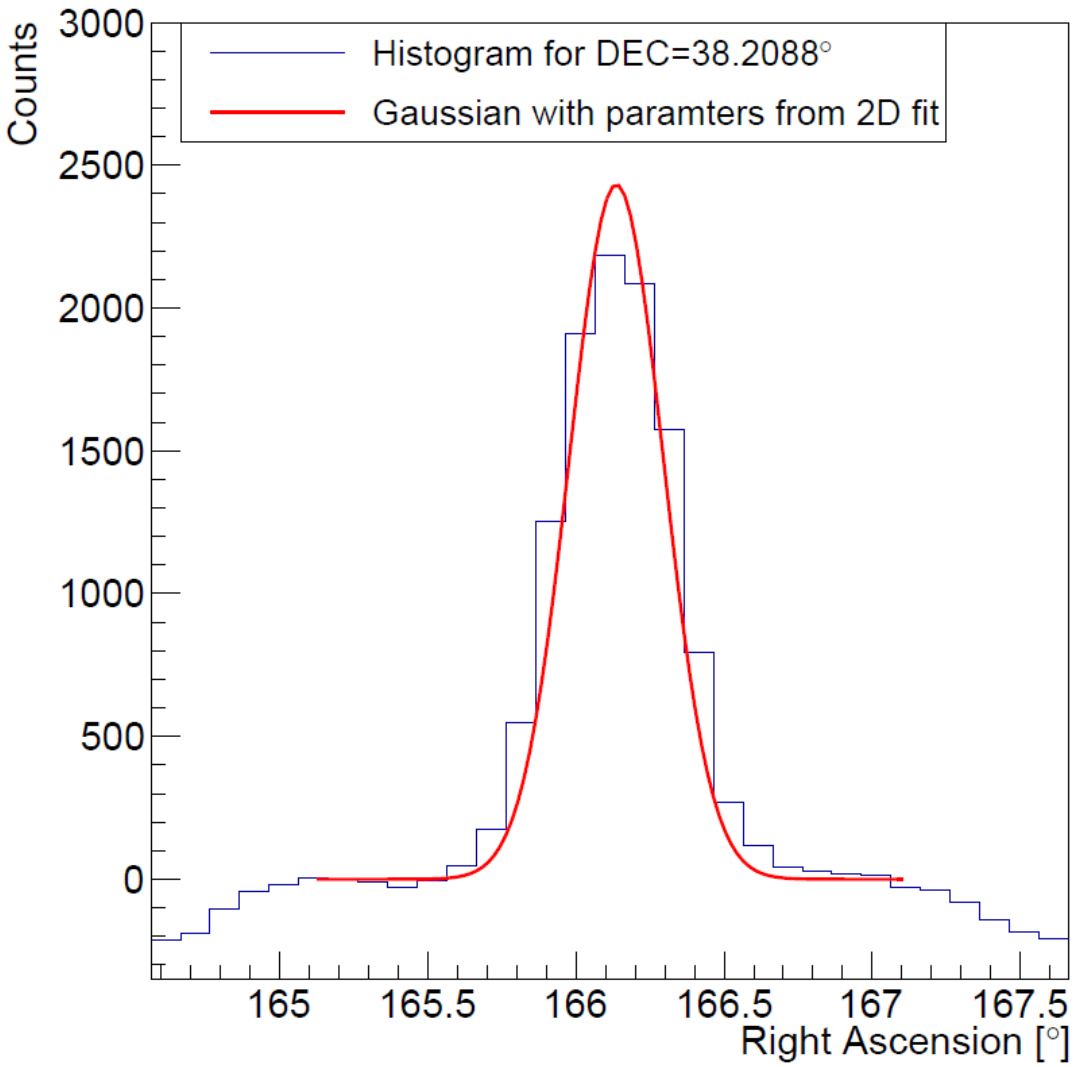

Figure 22: The counted events for the source Mrk421 are shown. This is done for 38.2088 ° DEC. Additionally, the corresponding part of the two-dimensional Gaussian fit is shown. No discrepancies can be observed.

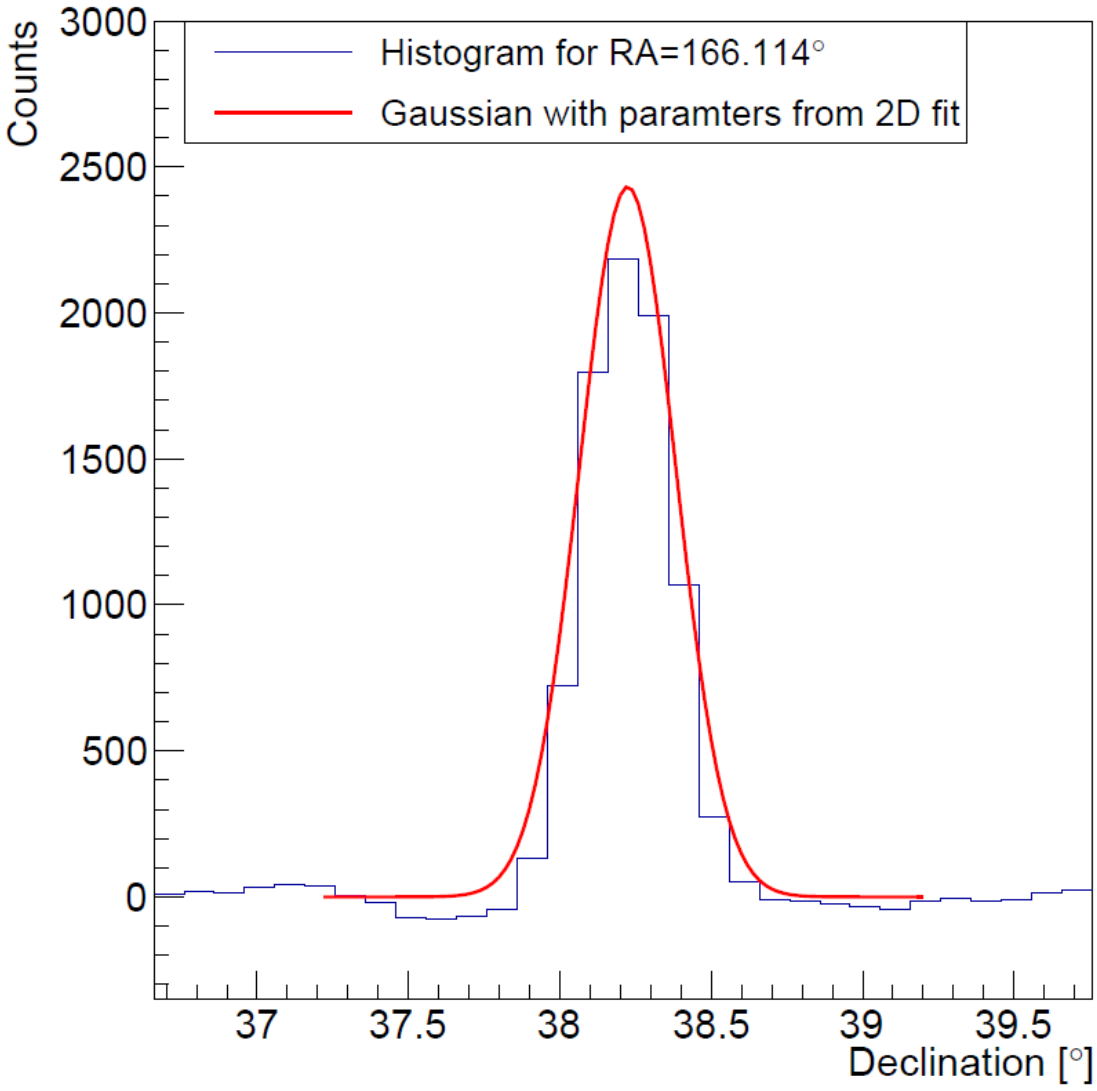

Figure 23: The counted events for the source Mrk421 are shown. This is done for 166.114 ° RA. Additionally, the corresponding part of the two-dimensional Gaussian fit is shown. No discrepancies can be observed.

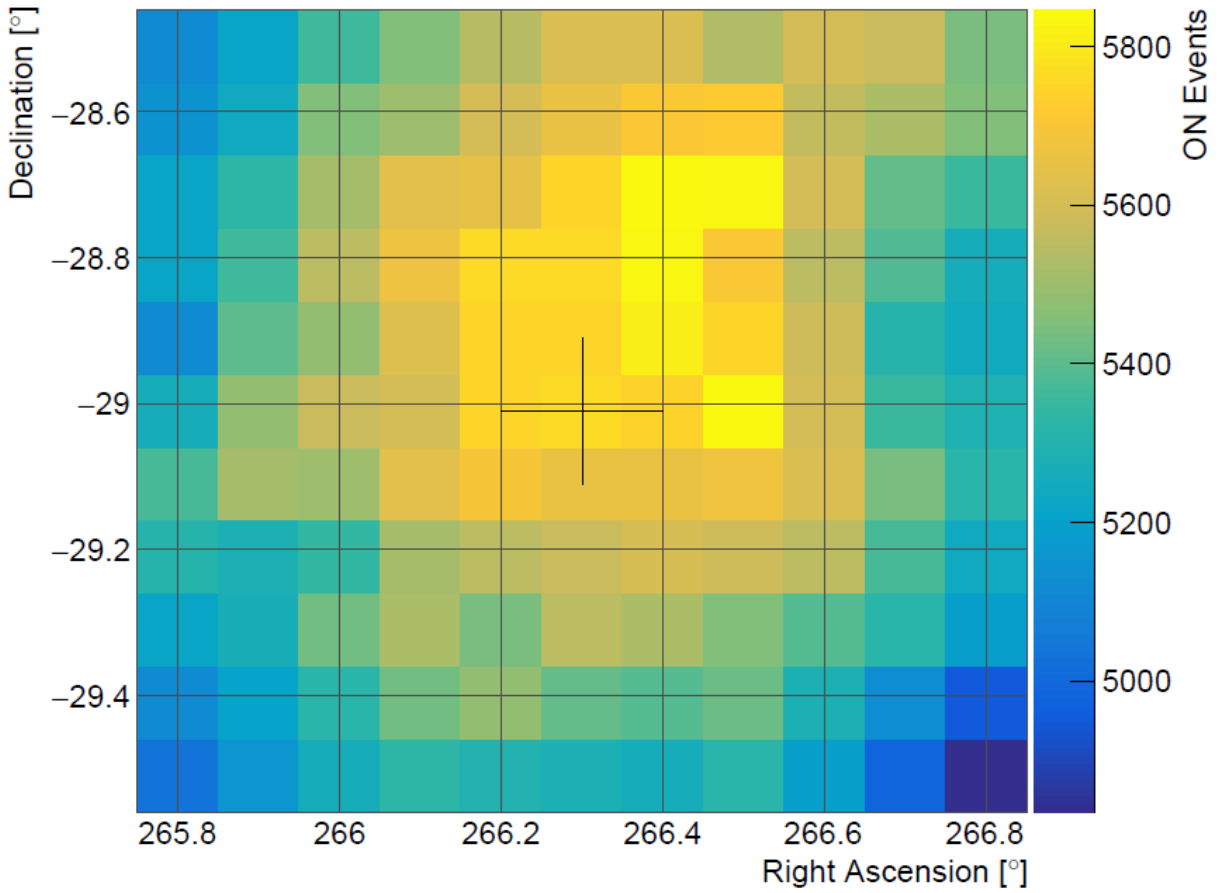

Figure 24: The area ($\pm 0.5\,^\circ$ in RA and DEC) around the galactic centre is visible. The position of the galactic centre is marked with a cross. The colour indicates the number of ON events for each position. For this skymap, about 33 h of data are analysed after the data quality selection. An extended area with a high number of ON events is visible.

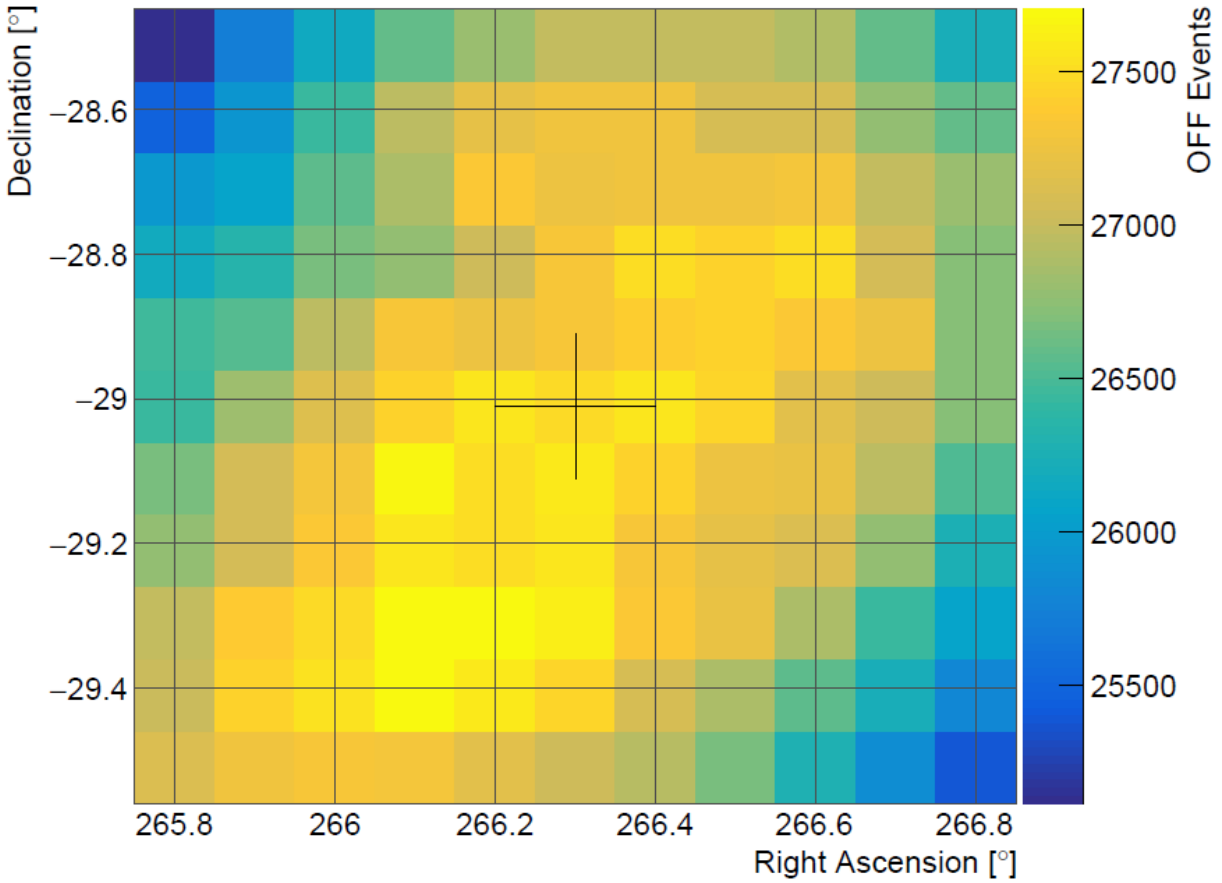

Figure 25: The area with $\pm 0.5^\circ$ in RA and DEC around the galactic centre is shown. The position of the galactic centre is marked with a cross. The colour indicates the number of OFF events for each position. The skymap consists of around 33 h of data, after the data quality selection. An extended area with a high number of OFF events is visible. Compared to the ON data, the bright part is extended into the lower left corner.

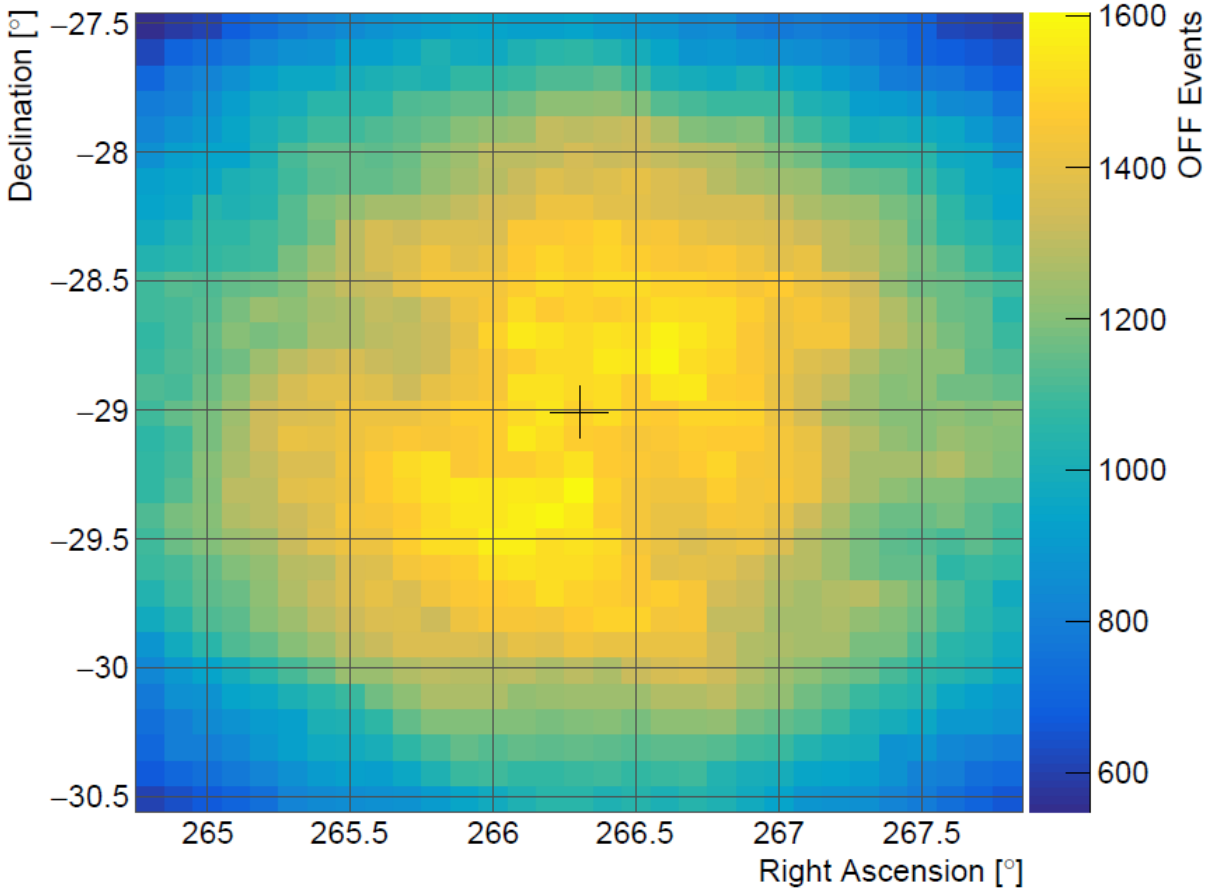

Figure 26: The area with $\pm 1.5^\circ$ in RA and DEC around the position of the galactic centre, marked with a cross, is shown. The color indicates the number of OFF events. About 2 h of data (after the data quality selection) are analysed for this skymap. A large defuse higher number of events is visible around the galactic centre.

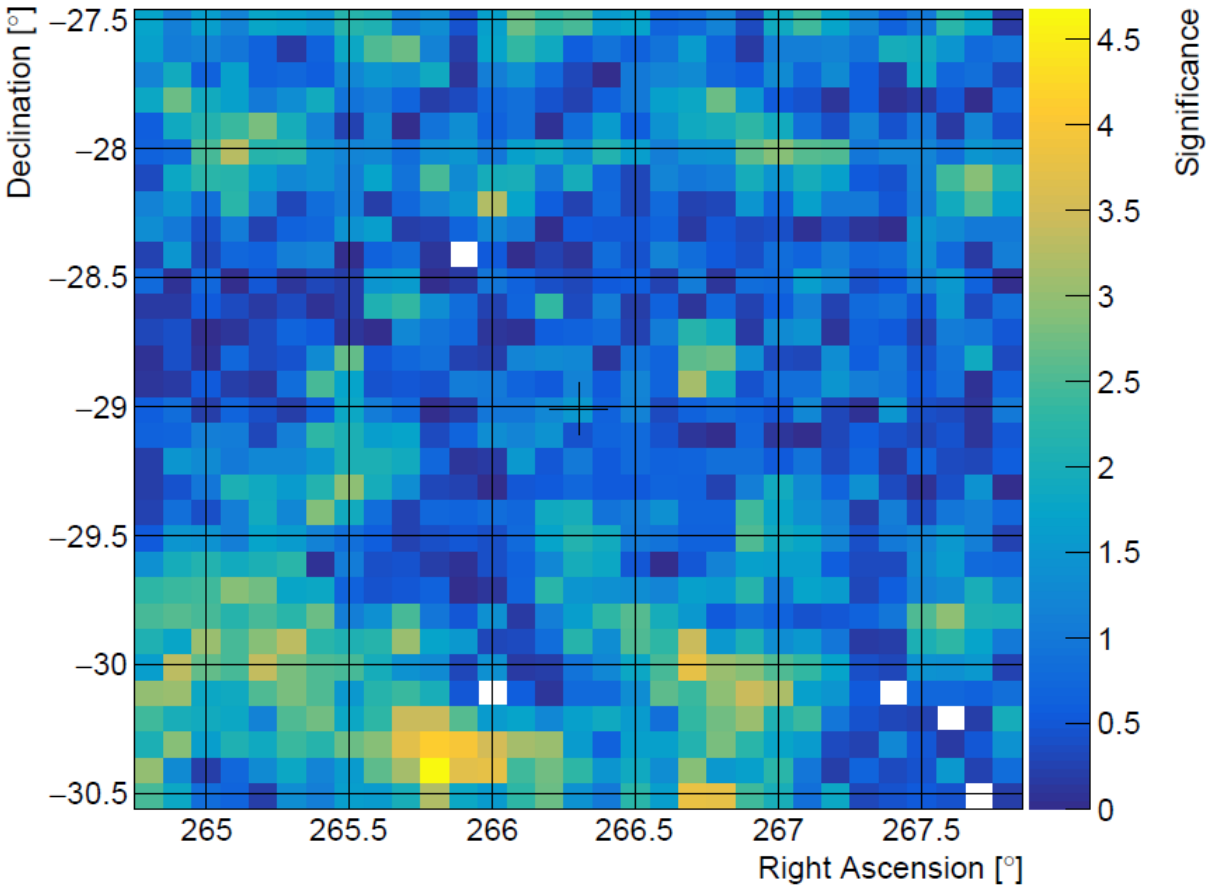

Figure 27: The area ($\pm 1.5^\circ$ in RA and DEC) around the galactic centre is visible. The position of the galactic centre is marked with a cross. The colour indicates the significance of each position. The skymap was created using 2 h of data (after the data quality selection). No source seems to be visible. The white squares are the position where the calculation of the significance failed.

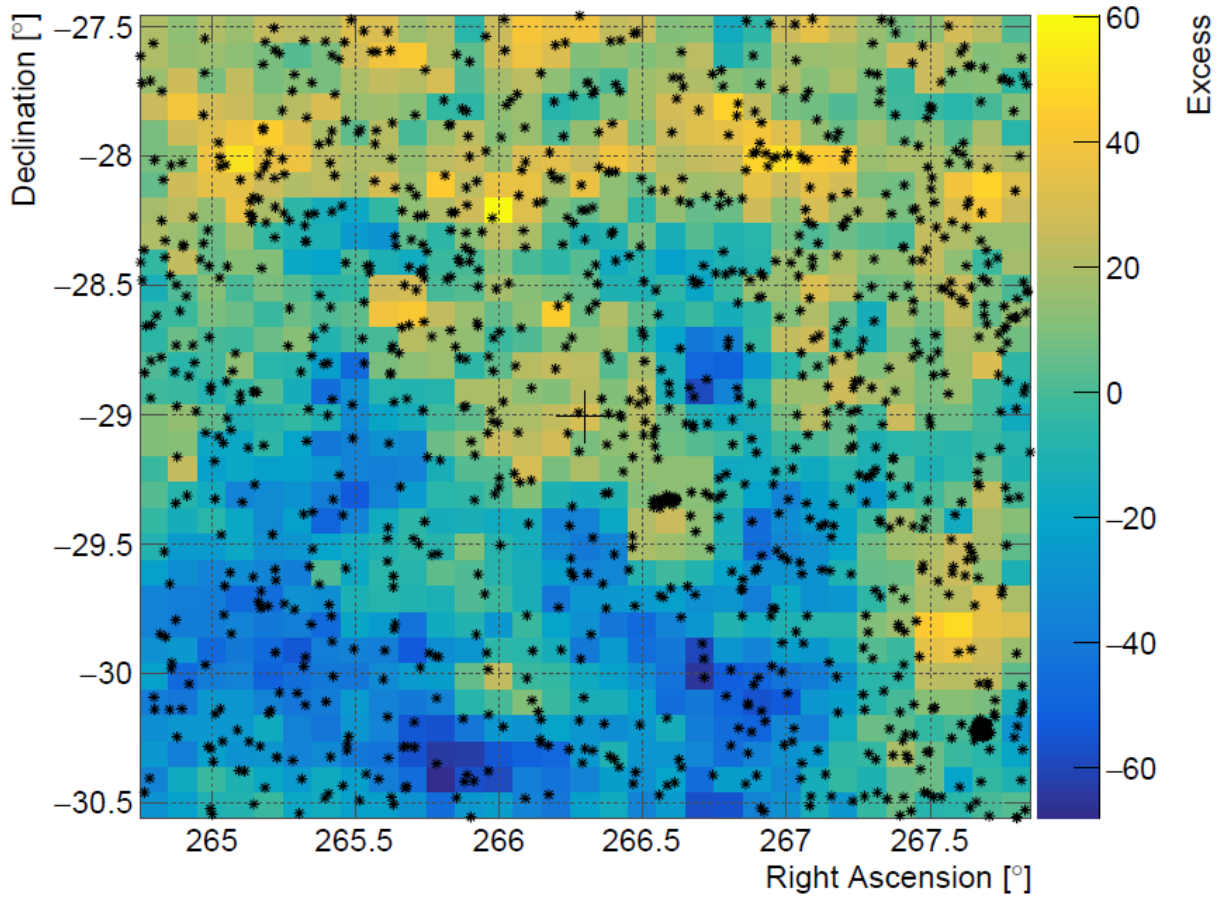

Figure 28: The area ($\pm 1.5^\circ$ in RA and DEC) around the galactic centre is visible. The position of the galactic center is marked with a cross. The colour indicates the excess for each position. 2 h of data are analyzed for this skymap. No source seems to be detected. The stars represent objects with a magnitude higher than 30 in the B-band. The information about the objects is from the SIMBAD database.

Declaration of originality

I declare that I have authored this thesis independently, that I have not used other than the declared sources / resources, and that I have explicitly marked all material which has been quoted either literally or by content from the used sources.

Würzburg, July 24, 2024 Name Name .....

References

Abdo, A. A. et al. (May 2012). "Observation and Spectral Measurements of the Crab Nebula with Milagro". In: 750.1, 63, p. 63. DOI: 10.1088/0004-637X/750/1/63. arXiv: 1110.0409 [astro-ph.HE].

Abeysekara, A. U. et al. (July 2017). "The 2HWC HAWC Observatory Gamma-Ray Catalog". In: 843.1, 40, p. 40. DOI: 10.3847/1538-4357/aa7556. arXiv: 1702.02992 [astro-ph.HE].

Adams, C. B. et al. (June 2021). "VERITAS Observations of the Galactic Center Region at Multi-TeV Gamma-Ray Energies". In: 913.2, 115, p. 115. DOI: 10.3847/1538-4357/abf926. arXiv: 2104.12735 [astro-ph.HE].

Albert, A. et al. (Apr. 2022). "Long-term Spectra of the Blazars Mrk 421 and Mrk 501 at TeV Energies Seen by HAWC". In: 929.2, 125, p. 125. DOI: 10.3847/1538-4357/ac58f6. arXiv: 2106.03946 [astro-ph.HE].

Aleksić, J. et al. (Jan. 2016). "The major upgrade of the MAGIC telescopes, Part II: A performance study using observations of the Crab Nebula". In: *Astroparticle Physics* 72, pp. 76–94. DOI: 10.1016/j.astropartphys.2015.02.005. arXiv: 1409.5594 [astro-ph.IM].

Anderhub, H. et al. (June 2013a). "Design and operation of FACT - the first G-APD Cherenkov telescope". In: *Journal of Instrumentation* 8.6, P06008, P06008. DOI: 10.1088/1748-0221/8/06/P06008. arXiv: 1304.1710 [astro-ph.IM].

— (June 2013b). "Design and operation of FACT - the first G-APD Cherenkov telescope". In: *Journal of Instrumentation* 8.6, P06008, P06008. DOI: 10.1088/1748-0221/8/06/P06008. arXiv: 1304.1710 [astro-ph.IM].

Arbet-Engels, A. et al. (Mar. 2021). "The relentless variability of Mrk 421 from the TeV to the radio". In: 647, A88, A88. DOI: 10.1051/0004-6361/201935557. arXiv: 2101.10651 [astro-ph.HE].

Beck, M. et al. (2019). "FACT - Probing the Periodicity of Mrk 421 and Mrk 501". In: *Proceedings of 36th International Cosmic Ray Conference — PoS(ICRC2019)*. Vol. 358, p. 630. DOI: 10.22323/1.358.0630.

Bikos, K. (n.d.). *Altitude Azimuth: The Horizontal Coordinate System*. https://www.timeanddate.com/astronomy/horizontal-coordinate-system.html [Accessed: 7 May 2024].

Bretz, T. (2019). "Zenith angle dependence of the cosmic ray rate as measured with imaging air-Cherenkov telescopes". In: *Astroparticle Physics* 111, pp. 72–86. ISSN: 0927-6505.

DOI: https://doi.org/10.1016/j.astropartphys.2019.02.004. URL: https://www.sciencedirect.com/science/article/pii/S0927650518302913.

Bretz, T. et al. (Dec. 2012). "FACT - The first G-APD Cherenkov telescope (first results)". In: *High Energy Gamma-Ray Astronomy: 5th International Meeting on High Energy Gamma-Ray Astronomy*. Ed. by Felix A. Aharonian, Werner Hofmann, and Frank M. Rieger. Vol. 1505. American Institute of Physics Conference Series. AIP, pp. 773–776. DOI: 10.1063/1.4772374.

Cornils, R. et al. (Nov. 2003). "The optical system of the H.E.S.S. imaging atmospheric Cherenkov telescopes. Part II: mirror alignment and point spread function". In: *Astroparticle Physics* 20.2, pp. 129–143. DOI: 10.1016/S0927-6505(03)00172-5. arXiv: astro-ph/0308247 [astro-ph].

Dorner, D. et al. (Jan. 2013). "FACTLong-term Monitoring of Bright TeV-Blazars". In: *International Cosmic Ray Conference*. Vol. 33. International Cosmic Ray Conference, p. 1093. DOI: 10.48550/arXiv.1311.0478. arXiv: 1311.0478 [astro-ph.HE].

— (Feb. 2015). "FACT - Monitoring Blazars at Very High Energies". In: *arXiv e-prints*, arXiv:1502.02582, arXiv:1502.02582. DOI: 10.48550/arXiv.1502.02582. arXiv: 1502.02582 [astro-ph.IM].

Evans, J. and Friedlander, M. W. (2024). *astronomy*. https://www.britannica.com/science/astronomy/Observations-of-the-galactic-centre [Accessed: 4 July 2024].

Hildebrand, D. et al. (2017). "Using Charged Cosmic Ray Particles to Monitor the Data Quality of FACT". In: *Proceedings of 35th International Cosmic Ray Conference — PoS(ICRC2017)*. Vol. 301, p. 779. DOI: 10.22323/1.301.0779.

Hrupec, D. (2008). *Extragalactic sources of rapidly variable high energy gamma radiation*. https://fulir.irb.hr/1517/1/319670.doctoralthesis.pdf [Accessed: 4 June 2024].

Lehrstuhl für Astronomie (2018). "Gamma-ray astronomy with the FACT telescope-Excess-rate curve of a TeV blazar". In: *Astronomische Methoden*.

Lessard, R. W. et al. (Mar. 2001). "A new analysis method for reconstructing the arrival direction of TeV gamma rays using a single imaging atmospheric Cherenkov telescope". In: *Astroparticle Physics* 15.1, pp. 1–18. DOI: 10.1016/S0927-6505(00)00133-X. arXiv: astro-ph/0005468 [astro-ph].

Li, T. -P. and Ma, Y. -Q. (Sept. 1983). "Analysis methods for results in gamma-ray astronomy." In: 272, pp. 317–324. DOI: 10.1086/161295.

López-Oramas, A. (Apr. 2015). "Multi-year Campaign of the Gamma-Ray Binary LS I +61∘ 303 and Search for VHE Emission from Gamma-Ray Binary Candidates with the MAGIC Telescopes". In: DOI: 10.13140/RG.2.1.4140.4969.

Lopez, M. et al. (July 2009). "Detection of the crab pulsar with MAGIC". In: *arXiv e-prints*, arXiv:0907.0832, arXiv:0907.0832. DOI: 10.48550/arXiv.0907.0832. arXiv: 0907.0832 [astro-ph.HE].

MAGIC Collaboration and Acciari, V. A. et al. (Oct. 2020). "MAGIC observations of the diffuse γ-ray emission in the vicinity of the Galactic center". In: 642, A190, A190. DOI: 10.1051/0004-6361/201936896. arXiv: 2006.00623 [astro-ph.HE].

Mahlke, M. et al. (2017). "FACT - Searching for periodicity in five-year light-curves of Active Galactic Nuclei". In: *Proceedings of 35th International Cosmic Ray Conference — PoS(ICRC2017)*. Vol. 301, p. 612. DOI: 10.22323/1.301.0612.

Pfahler, L., Bunse, M. and Morik, K. (Aug. 2021). *Noisy Labels for Weakly Supervised Gamma Hadron Classification*.

Schleicher, B. et al. (Mar. 2022). "FACT - Database-based Analysis and Spectrum Calculations". In: *37th International Cosmic Ray Conference*, 760, p. 760. DOI: 10.22323/1.395.0760.

Schönfelder, V. (2001). *The Universe in Gamma Rays*. Berlin: Springer-Verlag.

Seitz, M. et al. (2015). "Geometrical Reference Systems". In: *Handbook of Geomathematics*. Ed. by Willi Freeden, M. Zuhair Nashed, and Thomas Sonar. Berlin, Heidelberg: Springer Berlin Heidelberg, pp. 2995–3034. ISBN: 978-3-642-54551-1. DOI: 10.1007/978-3-642-54551-1_79. URL: https://doi.org/10.1007/978-3-642-54551-1_79.

The American Association of Variable Star Observers (n.d.). *Markarian 421*. https://www.aavso.org/vsots_mark421 [Accessed: 15 May 2024].

Weekes, T. C. (2003). *Very High Energy Gamma-Ray Astronomy*. Bristol: Institute of Physics Publishing.